Nonparametric inference of neutron star composition, equation of state, and maximum mass with GW170817

Reed Essick, Philippe Landry, and Daniel E. Holz

Phys. Rev. D **101**, 063007 — Published 5 March 2020

DOI: 10.1103/PhysRevD.101.063007

Nonparametric inference of neutron star composition, equation of state, and maximum mass with GW170817

Reed Essick*
Kavli Institute for Cosmological Physics, The University of Chicago, 5640 South Ellis Avenue, Chicago, Illinois, 60637, USA

Philippe Landry†
Enrico Fermi Institute and Kavli Institute for Cosmological Physics, The University of Chicago, 5640 South Ellis Avenue, Chicago, Illinois, 60637, USA and Gravitational-Wave Physics & Astronomy Center, California State University, Fullerton, 800 N State College Blvd, Fullerton, CA 92831

Daniel E. Holz‡
Enrico Fermi Institute, Department of Physics, Department of Astronomy and Astrophysics, and Kavli Institute for Cosmological Physics, The University of Chicago, Chicago, IL 60637, USA

(Dated: February 3, 2020)

The detection of GW170817 in gravitational waves provides unprecedented constraints on the equation of state (EOS) of the ultra-dense matter within the cores of neutron stars (NSs). We extend the nonparametric analysis first introduced in Landry & Essick (2019), and confirm that GW170817 favors soft EOSs. We infer macroscopic observables for a canonical $1.4\,M_\odot$ NS, including the tidal deformability $\Lambda_{1.4} = 211^{+312}_{-137}$ (491^{+216}_{-181}) and radius $R_{1.4} = 10.86^{+2.04}_{-1.42}$ ($12.51^{+1.00}_{-0.88}$) km, as well as the maximum mass for nonrotating NSs, $M_{\rm max} = 2.064^{+0.260}_{-0.134}$ ($2.017^{+0.238}_{-0.087}$) $M_\odot$, with nonparametric priors loosely (tightly) constrained to resemble candidate EOSs from the literature. Furthermore, we find weak evidence that GW170817 involved at least one NS based on gravitational-wave data alone ($B^{\rm NS}_{\rm BBH} = 3.3 \pm 1.4$), consistent with the observation of electromagnetic counterparts. We also investigate GW170817's implications for the maximum spin frequency of millisecond pulsars, and find that the fastest known pulsar is spinning at more than 50% of its breakup frequency at 90% confidence. We additionally find modest evidence in favor of quark matter within NSs, and GW170817 favors the presence of at least one disconnected hybrid star branch in the mass–radius relation over a single stable branch by a factor of 2. Assuming there are multiple stable branches, we find a suggestive posterior preference for a sharp softening around nuclear density followed by stiffening around twice nuclear density, consistent with a strong first-order phase transition. While the statistical evidence in favor of new physics within NS cores remains tenuous with GW170817 alone, these tantalizing hints reemphasize the promise of gravitational waves for constraining the supranuclear EOS.

I. INTRODUCTION

The observation of gravitational waves (GWs) from GW170817 [1], a coalescing compact binary with an electromagnetic counterpart, has greatly advanced the study of nuclear matter at extreme densities. Changes in the orbital phasing due to the components' mutual tidal interaction leave a detectable imprint in the GW signal [2–7], and several studies have exploited this fact to infer the tidal deformabilities of the compact objects involved in the coalescence [1, 8, 9]. The measured tidal deformabilities have, in turn, informed direct constraints on the equation of state (EOS) of neutron star (NS) matter [10–20]. Complementary astrophysical constraints have been supplied by observations of the gammay-ray burst and kilonova associated with GW170817 [21–31], electromagnetic measurements of neutron-star radii [32–35], and observations of massive pulsars [36–38]. The present constraints, dominated by the existence of $2\,M_\odot$ pulsars and the tidal constraints from GW170817, collectively point to an EOS that is relatively soft just above nuclear saturation density, so as to produce NSs with radii of less than ≈ 15 km, in line with nuclear-theoretic predictions from chiral effective field theory [39, 40], and stiff enough at higher densities to support the heaviest known NSs. However, because of the statistical uncertainties in the measurements of tides, radii and kilonova properties, inferences of finer features of the EOS are sensitive to the choice of prior, which must therefore be designed with care [9, 15, 29, 41–44].

Tighter and more robust constraints on the EOS will emerge as more observational data become available. As the advanced LIGO [45] and Virgo [46] detectors continue to operate, we can expect further observations of NS coalescences (e.g. Refs. [47, 48]) to add to our knowledge of the supranuclear EOS [5, 41, 49, 50]. More accurate NS radius measurements from pulse-profile modeling of accretion hotspots by NICER [51] and future x-ray obser-

* reedessick@kicp.uchicago.edu
† plandry@fullerton.edu
‡ holz@uchicago.edu

vatories [52–55] are also expected to advance the study of ultra-dense matter [56–59], as are the anticipated moment of inertia constraints from precision measurements of periastron advance in double NS systems [60–62] that will become possible when next-generation radio timing facilities [63–65] come online.

To maximize the amount of information that can be gleaned from present and future observations of NSs, an active campaign to develop improved methods for inferring the EOS from astrophysical observations has been underway for some time. Conceptually, the simplest way to learn about the EOS is to compare the evidence for different discrete candidate EOSs in a Bayesian framework [41, 66]. This, of course, is highly contingent on the EOSs made available by nuclear theorists and can yield no more than relative preferences. A more sophisticated approach is to infer the EOS directly by parameterizing it and determining the most likely parameters [49, 50, 67–69]. Parametric representations of the EOS range in complexity from constant sound-speed models [70–72] to piecewise polytropes [73, 74] and smooth spectral decompositions [75–78]. The next degree of sophistication dispenses with the parameterization altogether: inference of the EOS without artifical restrictions on its functional form is the aim of the *nonparametric inference*, which we further develop and apply in this paper.

Landry & Essick [15] (hereafter LE) recently introduced the first nonparametric method for inferring the NS EOS from GW observations based on Gaussian processes that automatically incorporate physical constraints, like causality and thermodynamic stability. We extend their methodology to investigate new questions in connection with GW170817, systematically testing hypotheses about the composition of ultra-dense matter and support for hybrid stars for the first time; establishing whether the event can be identified as a binary neutron star coalescence (as opposed to one involving a black hole) based on the GW data alone; and revisiting the consistency of observed pulsar spins with their rotational breakup frequencies in light of the EOS information from GW170817. We also obtain updated constraints on the EOS which reflect less ad-hoc prior choices and fuller representation of the body of candidate EOSs from nuclear theory than LE. Indeed, as LE and others (e.g., [9, 15, 29, 41–44]) have pointed out, prior choices can strongly impact the inferred EOS when we only have a few events. Our work, then, furthers the study of dense matter by optimizing the nonparameteric priors first introduced in LE as well as presenting several novel results that have not been previously quantified.

LE discussed the advantages of nonparametric analyses over parametric inference schemes with a finite number of parameters. Our updated analysis continues to avoid the kind of modeling systematics inherent to a coarse parametric representation of the EOS's unknown functional form [79], and we additionally improve the construction of the nonparametric EOS prior in several ways, reducing the impact of *ad-hoc* choices made within LE. Whereas LE chose hyperparameters for their Gaussian processes by hand when constructing their priors, we select them by finding hyperparameter sets that optimally reproduce the variability seen in a training set of candidate EOSs. We further sample over a mixture model of such sets, representing the overall process as a weighted sum over many individual Gaussian processes. Our priors, like LE's, naturally incorporate variable uncertainty in the EOS at different pressures, including tight constraints at low densities, where nuclear matter is better understood, and broader uncertainties at high densities. We also train our Gaussian processes on 50 tabulated candidate EOSs (as opposed to the 7 used in LE) and subdivide the resulting priors according to the composition of the EOSs on which they were trained. This elucidates finer-grained questions about NS composition while incorporating a broader range of theoretical expectations. Moreover, like Ref. [80], our analysis marginalizes over several possible crust EOSs to account for the (relatively small) uncertainty in the NS EOS at low densities. Leveraging this, we present new results based on the inferred posterior process for the EOS, including both posterior distributions for macroscopic observables associated with GW170817 itself and functional relations between generic NS observables.

Below, we briefly summarize our main conclusions. Consistent with previous studies [9, 13, 15, 66], we find that GW170817 favors relatively soft EOSs, assuming the system's components were both slowly spinning NSs [8]. This manifests as an overall posterior preference for lower pressures at and above nuclear density ($\rho_{\rm nuc} = 2.8 \times 10^{14}\,{\rm g/cm^3}$), as well as smaller radii (R), tidal deformabilities (Λ), and maximum masses for nonrotating NSs ($M_{\rm max}$). Our results are conditioned on the existence of $\approx 2\,M_\odot$ pulsars [37, 38] *a priori*, as we retain only EOSs drawn from our prior that support NSs of at least $1.93\,M_\odot$. All our conclusions, then, depend on GW and pulsar data, and our Bayes factors compare our GPs conditioned on both types of data to those conditioned only on pulsar observations. Like LE, we derive results using both *model-agnostic* and *model-informed* priors, reflecting different amounts of relative *a priori* confidence in candidate EOSs from the literature. Our *informed* prior is conditioned to closely emulate the behavior of EOSs proposed in the literature, whereas our *agnostic* prior generates much more diverse EOS behavior and is not tightly constrained by the EOS upon which it was conditioned. In this way, we investigate the relative preference of different theoretical behaviors with our *informed* priors while exploring the full set of causal and thermodynamically stable EOSs independent of specific theoretical predictions with our *agnostic* prior. With the *agnostic* (*informed*) prior, we infer median and 90% highest-probability-density credible regions for the macroscopic observables of a canonical $1.4\,M_\odot$ NS, namely $\Lambda_{1.4} = 211^{+312}_{-137}$ (491^{+216}_{-181}) and $R_{1.4} = 10.86^{+2.04}_{-1.42}$ ($12.51^{+1.00}_{-0.88}$) km, as well as $M_{\rm max} = 2.064^{+0.260}_{-0.134}$ ($2.017^{+0.238}_{-0.087}$) $M_\odot$, after marginalizing over

EOS composition. These results are broadly consistent with LE and other studies, but we note that our *informed* posteriors are nearly identical to the *informed* prior as the collection of nuclear-theoretic models used to condition that prior, while still quite diverse, spans only a small set of possible EOSs and constitutes a strong prior that dominates GW170817's likelihood.

Nonetheless, by constructing separate priors for different EOS compositions, our updated analysis shows that GW170817 weakly favors EOSs that contain quark matter: $P(\text{Quark}|\text{data}) = 56\%$ assuming equal prior odds for hadronic, hyperonic, and quark compositions with our *informed* prior. Remarkably, with the *agnostic* prior, we find that GW170817 modestly favors EOSs that support a disconnected hybrid star branch, one signature of a strong first-order phase transition. Among such EOSs, GW170817 suggests a possible phase transition with onset density between $\rho_{\rm nuc}$ and $2\rho_{\rm nuc}$, in agreement with chiral effective field theory predictions for the breakdown of perturbations away from asymmetric nuclear matter [39, 40, 43, 81]. Our nonparametric inference attaches no *a priori* significance to these particular densities; the preference observed *a posteriori* is entirely driven by data from GW170817 and $M_{\rm max}$ constraints from observations of massive pulsars. While these results are far from conclusive, they demonstrate the extent of information available from GW observations and hint at new physics within NS cores.

We also reexamine limits on NS spin based on the EOS, finding maximum dimensionless spins $\chi_{\rm max} \lesssim 0.5$ for masses $M \gtrsim M_\odot$. We find that the fastest known pulsar, J1748-2446ad [36], which does not have a precisely measured mass, rotates at $\gtrsim 1/2$ its breakup frequency for the same mass range at 90% confidence.

We additionally compute the relative marginal likelihoods for different progenitor systems, e.g. binary NS (BNS) vs. NS-black hole (NSBH), finding a preference for progenitor systems containing at least one NS compared to a binary BH (BBH) by a factor of 3.3 ± 1.4 while making minimal assumptions about the components' spins, in agreement with the observation of electromagnetic counterparts [82, 83]. Interestingly, we find a further slight preference for the lighter component to be a BH, with $B^{\rm NSBH}_{\rm BNS} = 1.87 \pm 0.61$ for our *agnostic* prior. This is likely due to GW170817 favoring relatively small Λ_2, which is slightly more consistent with a BH ($\Lambda_2 = 0$) than the large Λ_2 required by most NS EOSs.

As with LE, our *agnostic* and *informed* results bracket other results in the literature. For example, Ref. [13] constrained the radii of each of GW170817's components to be $11.9^{+1.4}_{-1.4}$ km, while Ref. [9] assumed $R_1 = R_2$ and found a radius of 8.9–13.2 km. Similarly, Ref. [8] constrained $\tilde{\Lambda} = 300^{+420}_{-230}$ and Ref. [9] found $\tilde{\Lambda} = 222^{+420}_{-138}$ assuming a uniform component mass prior. We infer $\tilde{\Lambda} = 245^{+361}_{-160}$ (572^{+254}_{-212}) with the *agnostic* (*informed*) prior. Although no previous constraints on NS composition are available, we note that Ref. [66] calculated Bayes factors between BNS and BBH models for individual candidate EOSs, with $\ln B^{\rm BNS}_{\rm BBH} \lesssim 2$ in all cases using a broad mass prior and the majority of candidate EOSs yielding $\ln B^{\rm BNS}_{\rm BBH} \sim 0$. This is in good agreement with our *agnostic* estimate of $\ln B^{\rm BNS}_{\rm BBH}(\chi_i \leq 0.89) = 0.85 \pm 0.69$. Therefore, where comparable, our findings are generally in good agreement with existing results in the literature.

We review the nonparametric inference introduced in LE in Section II, including descriptions of our improvements. Section II A describes the priors constructed for this work. Using publicly available posterior samples [84] from a study of GW170817's source properties [8], Section III presents *a posteriori* constraints obtained for macroscopic observables associated with GW170817, such as the component masses and tidal deformabilities, while Section IV presents constraints for relationships between macroscopic observables, applicable to systems besides GW170817. Section V describes our inference over NS compositions, and we conclude in Section VI.

II. NONPARAMETRIC INFERENCE OF THE EQUATION OF STATE

We extend the nonparametric inference based on Gaussian processes (GPs) detailed in LE, and refer readers to that paper for a pedagogical introduction to GPs, their use in our analysis, and associated notation. Nonetheless, we provide a brief overview in what follows.

A GP assumes Gaussian correlations between functional degrees of freedom, described by a mean and covariance. By conditioning a joint process on the observed data and assuming a functional form for the covariance, we obtain a process for infinitely many degrees of freedom based on a finite set of known data, and the complexity of the resulting nonparametric model can naturally scale with the amount of available data. A thorough description is available in Ref. [85], but the key insight is that the probability distribution of a functional degree of freedom (f) given a corresponding abscissa (x) and known data (f_*, x_*) is

$$P(f|f_*, x, x_*; \vec{\sigma}) = \frac{P(f, f_*|x, x_*; \vec{\sigma})}{P(f_*|x_*; \vec{\sigma})} \tag{1}$$

assuming

$$P(f, f_*|x, x_*, \vec{\sigma}) = \mathcal{N}\big(\mu(x_i), K(x_i, x_j; \vec{\sigma})\big), \tag{2}$$

where $\mu(x_i)$ is the mean and $K(x_i, x_j; \vec{\sigma})$ the covariance of a multivariate normal distribution. K is a function of the *hyperparameters* $\vec{\sigma}$. We use the squared-exponential kernel

$$K_{\rm se}(x_i, x_j; \sigma, l) = \sigma^2 \exp\left(-\frac{(x_i - x_j)^2}{2l^2}\right), \tag{3}$$

which models correlations between neighboring functional degrees of freedom, the white-noise kernel

$$K_{\rm wn}(x_i, x_j; \sigma_{\rm obs}) = \sigma_{\rm obs}(x_i)\delta(x_i - x_j), \tag{4}$$

which models uncertainty at each point, and a scaled covariance between input models

$$K_{\rm mv}(x_i, x_j; m) = m^2 \left(\frac{1}{N_A} \sum_{a \in A} C_{ij}^{(a)} + \frac{1}{N_A} \sum_{a \in A} \left(\mu_i^{(a)} - \bar{\mu}_i^{(A)} \right) \left(\mu_j^{(a)} - \bar{\mu}_j^{(A)} \right) \right) \quad (5)$$

where A is the set of N_A input models, $\mu^{(a)}$ and $C^{(a)}$ are the mean and covariance of the process for model a,

$$\bar{\mu}_i^{(A)} = \frac{1}{N_A} \sum_{a \in A} \mu_i^{(a)}, \quad (6)$$

and m scales the relative importance of this model covariance. $K_{\rm mv}$, like $K_{\rm wn}$, represents theoretical uncertainty. We note that LE used a simplified version of $K_{\rm mv}$ which only included the diagonal components of the covariance matrix.

We generate GPs for an auxiliary variable

$$\phi = \log \left(c^2 \frac{d\varepsilon}{dp} - 1 \right) \quad (7)$$

conditioned on tabulated EOSs from the literature, where ε is the total energy density and p the pressure. Any realization of ϕ will automatically satisfy both causality and thermodynamic-stability constraints ($0 \leq c_s^2 = dp/d\varepsilon \leq c^2$). Our method employs GPs for two main purposes: mapping irregularly sampled tabulated data for $\varepsilon(p)$ into a regularly sampled process for $\phi(p)$ while self-consistently computing the uncertainty in that mapping, and emulating the behavior seen in tabulated EOSs to generate synthetic EOSs which resemble models from the literature. This work differs from LE in that we construct mixture models of GPs instead of relying on a single set of hyperparameters. That is,

$$\phi \sim \sum_i w_i P(\phi | \vec{\sigma}_i) \quad (8)$$

where $\vec{\sigma}_i$ and w_i are the hyperparameters and weight associated with the $i^{\rm th}$ element of the mixture model.

We constrain our processes to approximately match known low-pressure physics with an additional white-noise variant. This forces all realizations of the conditioned process to approach a constant value (chosen to be $\phi \to \phi_0 = 6$ based on `sly` [86]) with a white-noise scaling parameter

$$\sigma_{\rm obs}(p) = \left(\frac{p}{p_{\rm ref}} \right)^n. \quad (9)$$

At low pressures, $\sigma_{\rm obs} \to 0$, forcing the conditioned process to approach ϕ_0 while imposing no constraint when $p \gg p_{\rm ref}$. Here we set $p_{\rm ref} = 5.4 \times 10^{31}\,{\rm dyn/cm^2}$ and $n = 5$, *ad hoc* choices with negligible impact on the resulting EOS, as we match the GP realizations onto a fixed model for the low-density crust well above $p_{\rm ref}$ [87]. Below the matching point, typically $\gtrsim 0.1\rho_{\rm nuc}$, our synthetic EOSs follow the crust. Improved matching conditions that incorporate the expected uncertainty from first-principles theoretical calculations, such as those in Refs. [39, 81, 88, 89], may further enhance our analysis. Similarly, matching to known high-density behavior, like $c_s^2 \to c^2/3$ for hyperrelativistic matter [90, 91], could prove interesting. However, we leave this to future work.

In addition to these technical improvements, we extend LE's analysis by conditioning our GPs on more tabulated EOSs (50 instead of 7) with a broader range of phenomenology and compositions. We also subdivide our *agnostic* and *informed* priors according to the composition of the input candidate EOSs (hadronic $npe\mu$ matter, hyperonic $npe\mu Y$ matter, or $npe\mu(Y)Q$ quark matter) allowing for model selection between different NS constituents.

A. Constructing nonparametric priors

We construct several priors using the candidate EOSs listed in Table VII. In order to fairly weight the importance of each input EOS, we group them by composition and underlying family of nuclear effective forces, generating a representative process for each family separately and then weighing the resulting GPs equally. This is done hierarchically in order to synthesize overarching *agnostic* and *informed* priors, as well as priors that demonstrate behavior characteristic of EOSs with a particular composition.

We map ε to ϕ for each EOS, modeling each one's covariance matrix separately with a squared-exponential kernel with a small white-noise term ($\sigma \gg \sigma_{\rm obs}$), and then generate a sequence of overarching GPs which emulate the behavior observed between different EOSs using a combination of squared-exponential, white-noise, and model covariance kernels. As in LE, we take the mean of the joint process before conditioning to be a low-order polynomial fit to the input data.

We optimize the hyperparameters used to generate our priors with a cross-validation likelihood

$$P_{\rm CV}(\{\varepsilon\}_A | p, \vec{\sigma}) = \prod_{a \in A} P(\varepsilon^{(a)} | \{\varepsilon\}_{A \setminus a}, p, \vec{\sigma}), \quad (10)$$

where $\{\varepsilon\}_A$ is the set of all EOSs and $\{\varepsilon\}_{A \setminus a}$ is the set of all EOSs in A except $\varepsilon^{(a)}$, and obtain processes that emulate the behavior seen within each composition separately. However, instead of selecting a single set of optimal hyperparameters for each composition, we instead create mixture models by drawing many sets of hyperpa-

rameters from $P_{\rm CV}$ so that

$$\begin{aligned} P(\varepsilon|\{\varepsilon\}_A, p) &\propto \int d\vec{\sigma}\, P(\vec{\sigma}) P_{\rm CV}(\{\varepsilon\}_A|\vec{\sigma})^\beta P(\varepsilon|\{\varepsilon\}_A, p, \vec{\sigma}) \\ &\approx \frac{1}{N}\sum_i P_{\rm CV}(\{\varepsilon\}_A|\vec{\sigma}_i)^\beta P(\varepsilon|\{\varepsilon\}_A, p, \vec{\sigma}_i) \quad \Big| \quad \vec{\sigma}_i \sim P(\vec{\sigma}) \end{aligned} \tag{11}$$

where $\beta = 1/T$ is an inverse temperature.

In the limit $T \to 1$, we weight each set of hyperparameters by the cross-validation likelihood. We call the resulting GP mixture model the *model-informed* prior. In the limit $T \to \infty$, we weight each set of hyperparameters equally, subject to the hyperprior $P(\vec{\sigma})$. This produces a process much less constrained by the input EOSs, which we refer to as the *model-agnostic* prior. We sample logarithmically in σ, $\sigma_{\rm obs}$, and m while sampling linearly in l. The precise choice of $P(\vec{\sigma})$ does not strongly affect the *model-informed* prior, but can modify the behavior of the *model-agnostic* prior. It is also worth noting that β provides a natural way to tune the *a priori* degree of belief placed on published theoretical models, and our choices for the *informed* and *agnostic* priors are not the only ones possible. Nonetheless, our *informed* prior emulates the observed behavior of nuclear-theoretic EOSs within the density range relevant for GW170817, while our *agnostic* prior explores the full set of causal and thermodynamically stable EOSs. Example synthetic EOSs are shown Figure 1.

B. Sampling from nonparametric priors

We obtain a large number of synthetic EOSs by sampling from each process for ϕ. We integrate each realization $\phi^{(\alpha)}(p)$ to obtain the associated synthetic EOS $\varepsilon^{(\alpha)}(p)$. This includes setting the initial value for the integration, which is done by matching to a crust EOS at a particular pressure. To marginalize over the (relatively small) theoretical uncertainty in the microscopic description of the crust, we randomly match each $\varepsilon^{(\alpha)}$ to the low-density model used in one of either `sly` [86], `eng` [92], or `hqc18` [93]. Furthermore, the precise pressure at which we match the crust EOS is allowed to vary by approximately an order of magnitude. This procedure generates EOSs which span all densities relevant for NS structure.

We integrate each synthetic EOS to obtain the corresponding relationships between macroscopic observables, such as the mass, radius, and tidal deformability. As in LE, we additionally require that each $\varepsilon^{(\alpha)}$ support a star of at least $1.93\,M_\odot$ based on the existence of massive pulsars (namely J0348+0432 [37]), discarding any synthetic EOS that does not. We also discard any EOS that supports a spurious branch of NSs with $M \gtrsim M_\odot$ at subnuclear densities $\rho_c < 0.8\rho_{\rm nuc}$, so as to exclude particularly large excursions in pressure just above the crust-core interface. We obtain marginal likelihoods, posterior distributions, and posterior processes by Monte-Carlo sampling from the prior representing a specific hypothesis, $\mathcal{H}$, weighting each sample with a Gaussian kernel density estimate (KDE) for the GW likelihood, $\mathcal{L}(\text{data}|\cdots)$, generated with publicly available samples [84]:

$$P(d|\varepsilon^{(\alpha)}, \mathcal{H}) = \int dM_1 dM_2\, p(M_1, M_2|\mathcal{H})\, \mathcal{L}\left(\text{data}\,\middle|\, M_1, M_2, \Lambda^{(\alpha)}(M_1), \Lambda^{(\alpha)}(M_2)\right) \tag{12}$$

$$\approx \frac{1}{N_i}\sum_i^{N_i} \mathcal{L}\left(\text{data}\,\middle|\, M_1^{(i)}, M_2^{(i)}, \Lambda^{(\alpha)}(M_1^{(i)}), \Lambda^{(\alpha)}(M_2^{(i)})\right) \quad \Big| \quad M_1^{(i)}, M_2^{(i)} \sim P(M_1, M_2|\mathcal{H})\,, \tag{13}$$

where $\Lambda^{(\alpha)}$ is the mass-tidal deformability relation implicitly defined by $\varepsilon^{(\alpha)}$. It is worth noting that several sets of samples are publicly accessible. Our specific choice is not expected to significantly affect our conclusions, although our precise quantitative results will depend on issues like waveform systematics discussed in Ref. [94]. Drawing $\varepsilon^{(\alpha)}$ from our prior and associating this marginal likelihood with each sample generates the posterior process. This also allows us to immediately estimate the evidence for each prior, up to a common normalization constant:

$$P(d|\{\varepsilon\}_A, \mathcal{H}) \approx \frac{1}{N_\alpha}\sum_\alpha^{N_\alpha}\frac{1}{N_i}\sum_i^{N_i} \mathcal{L}\left(\text{data}\,\middle|\, M_1^{(i)}, M_2^{(i)}, \Lambda^{(\alpha)}(M_1^{(i)}), \Lambda^{(\alpha)}(M_2^{(i)})\right) \quad \Big| \quad \begin{matrix} M_1^{(i)}, M_2^{(i)} \sim P(M_1, M_2|\mathcal{H}) \\ \varepsilon^{(\alpha)} \sim P(\varepsilon|\{\varepsilon\}_A) \end{matrix}\,, \tag{14}$$

where we draw N_i mass realizations for each of the N_α EOS realizations. Within this Monte-Carlo algorithm,

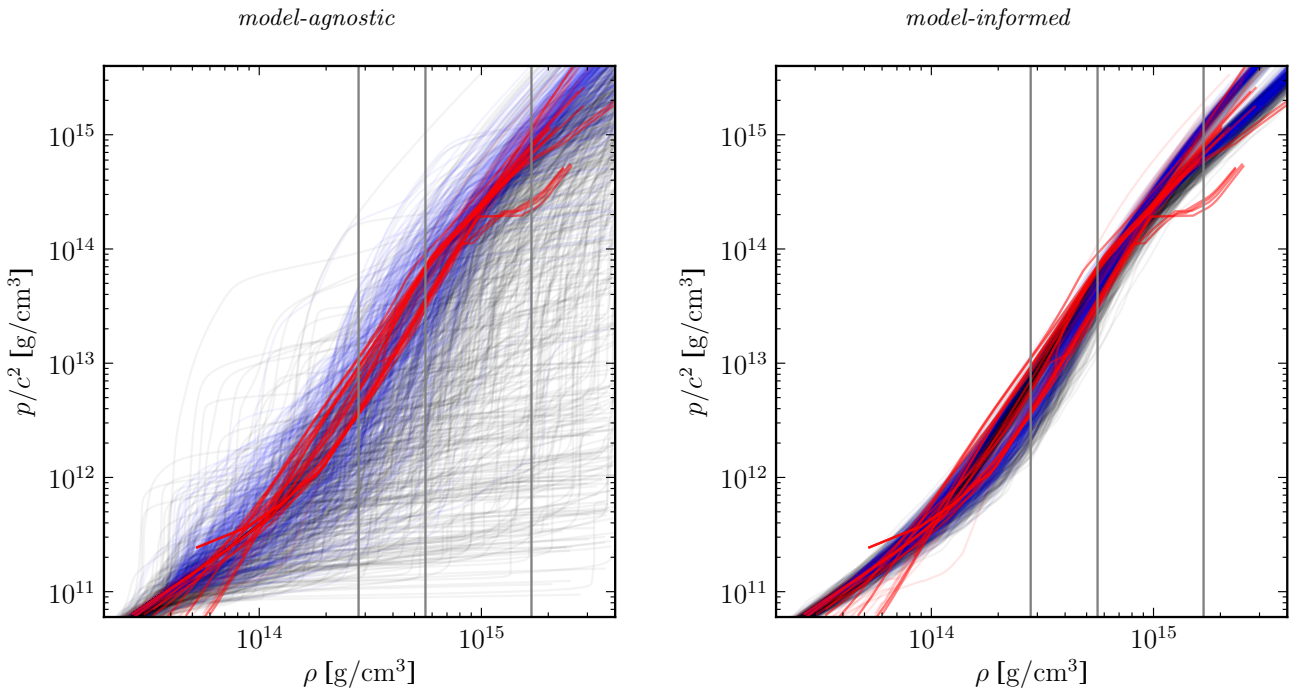

FIG. 1. Example synthetic EOSs drawn from our (*left*) *agnostic* and (*right*) *informed* nonparametric priors, constructed as mixture models with equal prior odds for hadronic, hyperonic, and quark compositions. Draws from the prior are colored according to the maximum nonrotating NS mass they support: *blue* for $M_{\rm max} \geq 1.93\,M_\odot$, and *black* otherwise. Candidate EOSs from the literature, used as input for our GPs, are shown in *red* (see Table VII). Vertical lines indicate once, twice and six times nuclear saturation density.

we optimize our KDE model for $\mathcal{L}(d|\cdots)$ by selecting bandwidths that maximize a cross-validation likelihood based on the public samples (see Appendix B).

The overarching composition-marginalized priors are constructed hierarchically, assuming equal prior odds for each composition, which is to say

$$P(\text{data}|X) = \frac{1}{3}\big[P(\text{data}|X;\text{Hadronic}) + P(\text{data}|X;\text{Hyperonic}) + P(\text{data}|X;\text{Quark})\big] \quad (15)$$

for *informed* and *agnostic* priors processes separately. In the following sections, we analyze GW170817 using both our *agnostic* and *informed* priors. The full set of results, broken down by composition, is given in Appendix D. Indeed, our *informed* posteriors essentially recover the *informed* priors, as is likely the case for all priors strongly informed by nuclear theory.

III. IMPLICATIONS FOR GW170817

We apply publicly available GW data from GW170817 [84] to our priors to infer the system's properties *a posteriori*. Section III A focuses on macroscopic observables associated with the inspiral stage of the coalescence, such as component masses ($M_{1,2}$), tidal deformabilities ($\Lambda_{1,2}$), and radii ($R_{1,2}$), while Section III B focuses on the nature of the progenitor system and the remnant. Throughout this section, we quote medians and 90% highest-probability-density credible regions unless otherwise stated.

A. Constraints on GW170817's macroscopic observables

We begin with posterior constraints on the macroscopic properties of GW170817, assuming both compact objects were slowly spinning NSs. Table I enumerates credible regions for various properties of GW170817's constituents, and Figure 2 demonstrates the correlations between some of these properties. In principle, our inference constrains any EOS-dependent observable associated with the event, but we focus on those that either directly impact the GW waveform or have been discussed extensively elsewhere in the literature. While we show low-dimensional projections of our data, we perform our inference in the four-dimensional space spanned by M_1, M_2, Λ_1, and Λ_2, and therefore posterior constraints may not be intuitive from the the low-dimensional projections in our figures.

We analyze publicly available posterior samples [95] with component spins constrained to be below 0.05 [84],

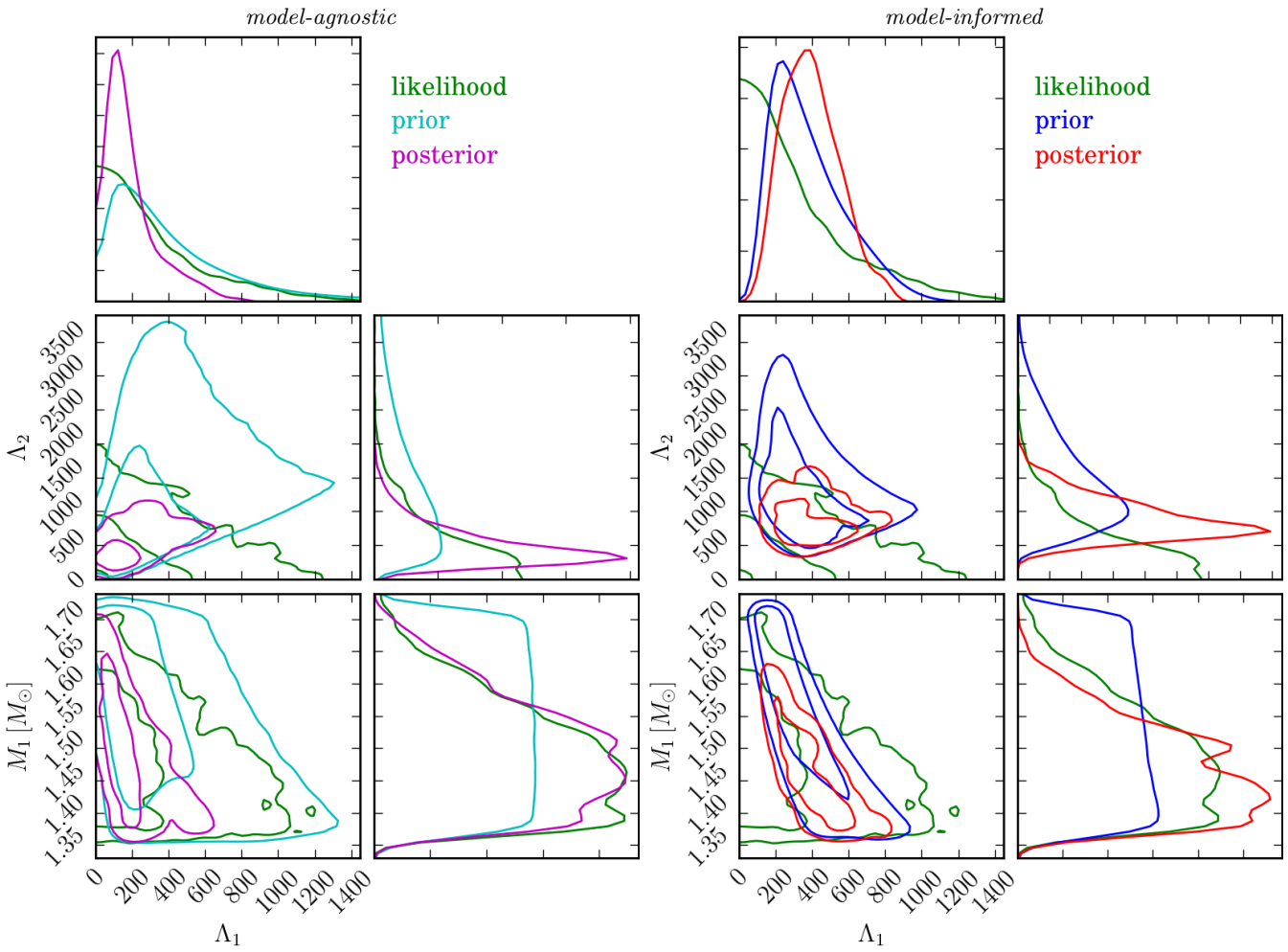

FIG. 2. Distributions for M_1, Λ_1, and Λ_2 after marginalizing over NS composition. (*Left*) *model-agnostic* prior (*cyan*), posterior (*magenta*), and low-spin marginal likelihood (*green*). (*Right*) *model-informed* prior (*blue*), posterior (*red*), and low-spin marginal likelihood (*green*). Contours in the joint distributions denote highest-posterior-density 50% and 90% credible regions.

and $\gtrsim O(10^5)$ synthetic EOSs drawn from each of our priors with 50 mass realizations per EOS. We find that relative uncertainties obtained with the *informed* prior are generally smaller than those with the *agnostic* prior, although the distributions of some parameters, like tidal deformabilities, are centered on larger values with the *informed* prior and can produce larger credible intervals in absolute terms. The inferred component mass distributions do not depend strongly on the EOS prior assumed, although they do change slightly *a posteriori* because they are correlated with the tidal deformability and radius, which are more sensitive to EOS assumptions. Specifically, the *agnostic* prior supports extreme EOSs and produces rather low values for Λ and R *a posteriori*. The *informed* prior prefers stiffer EOSs and yields correspondingly larger Λ and R. Table I lists the precise credible regions obtained. We note that the inferred tidal deformabilities are consistent with LE, and both the Λ and R credible regions are consistent with others in the literature. In particular, Ref. [13] constrained R_1 and R_2 separately, finding both to be $11.9^{+1.4}_{-1.4}$ km, while Ref. [9] assumed a common radius for the NSs and constrained it to 8.9–13.2 km. We find $R_1 = 10.88^{+1.99}_{-1.37}$ km and $R_2 = 10.82^{+2.14}_{-1.55}$ km with our *agnostic* prior, confirming the validity of the common radius assumption *a posteriori*. Similarly, Ref. [8] finds $\tilde{\Lambda} = 300^{+420}_{-230}$, while Ref. [9] quotes $\tilde{\Lambda} = 222^{+420}_{-138}$ for a uniform component mass prior. Our *agnostic* prior yields $\tilde{\Lambda} = 245^{+361}_{-160}$ [96]. Finally, our constraints remain marginally consistent with those quoted in Refs. [22, 24–26] based on electromagnetic observations, which set a lower bound of $\tilde{\Lambda} \gtrsim 300$ (see Ref. [29] for a critical examination of these results).

Like Figure 1 in Ref. [13] and Figure 6 in LE, Figure 2 shows the prior, likelihood, and posterior credible regions for M_1, Λ_1, and Λ_2 with our composition-marginalized priors. The preference for softer EOSs in the *agnostic* prior, both *a priori* and *a posteriori*, is readily apparent, as is the fact that the *agnostic* prior encompasses a wider

range of possibilities than the *informed* prior.

Table I also reports credible intervals for the central densities of the two components. These are consistent with those reported in both LE and Ref. [13]. We again note the general trend that the *agnostic* prior prefers softer EOSs with correspondingly compact stars containing denser cores and higher central pressures.

As discussed in LE, we obtain different *a posteriori* credible regions with different priors. However, neither of our priors are strongly favored by the data, with a Bayes factor of $B^{\mathcal{A}}_{\mathcal{I}} = 1.7952 \pm (1.1 \times 10^{-3})$ between them. This constitutes marginal evidence in favor of the *agnostic* priors over the *informed* priors, but serves mainly to demonstrate that posterior constraints on macroscopic observables and the EOS need to be interpreted with care, giving consideration to the underlying prior assumptions.

B. Implications for GW170817's progenitor and remnant

Section III A's results implicitly assume both constituents are NSs. This is reasonable given the masses involved, which are well below the minimum $M_{\rm max}$ allowed in our priors, and the electromagnetic counterparts observed in coincidence [82, 83]. However, we also consider the possibility that either (or both) of the constituents could be a BH. Although credible regions similar to Section III A could be derived for each case, we simply focus on the evidence for each progenitor type to determine whether the GW data alone can rule out the presence of at least one BH in the system.

Our evidence calculation involves Monte-Carlo integrals over a KDE representation of $\mathcal{L}(d|\cdots)$ along boundaries where Λ_1, $\Lambda_2 \to 0$. Such boundaries can introduce biases in the KDE representation of $\mathcal{L}$. After optimizing our KDE, we find that these effects introduce percent-level systematics.

We begin by investigating the nature of the progenitor system: did it consist of two NSs (BNS), a NS and a lighter BH (NSBH), a NS and a heavier BH (BHNS), or two BHs (BBH)? Table II quotes the posterior probability of each progenitor type assuming equal prior odds. We include results assuming both the low- and high-spin priors from Ref. [8], although the low-spin prior is motivated by the maximum observed rotation frequencies of pulsars in galactic BNS systems that will merge within a Hubble time (namely J0737–3039A [97] and J1946+2052 [98]) and may not be applicable to BHs. We also test for the presence of at least one NS. We find that GW170817 is relatively inconsistent with a BBH based on GW data alone, disfavored by a factor of 3.3 ± 1.4 relative to a progenitor with at least one NS with the high-spin *agnostic* prior, assuming $P(\text{BNS}) = P(\text{NSBH}) = P(\text{BHNS}) = 1/6$ and $P(\text{BBH}) = 1/2$. The weak preference for the BNS model with our *agnostic* prior is likely due to the relatively large Occam factor incurred by the extra freedom associated with $\Lambda_{1,2}$ compared to the BBH model. Therefore, even though the maximum likelihood within the BNS model is consistently four times larger than in the BBH model, the marginal likelihoods are comparable. This is also true to a lesser extent with the *informed* prior, but its stricter *a priori* assumptions also reduce the maximum likelihood and therefore the marginal evidence for the BNS model. In addition, of the possible progenitors containing a NS, GW170817 data weakly favor a NSBH, with $B^{\rm NSBH}_{\rm BNS}(\chi_i \leq 0.89,\ \textit{agnostic}) = 1.87 \pm 0.61$. This is likely due to marginally better matches to the data when $\Lambda_2 \to 0$ compared to the larger $\Lambda(M_2)$ required by our priors, instead of just an Occam factor, since NSBH models are preferred over BHNS models despite both having approximately equal prior volumes. We obtain qualitatively similar results with the high- and low-spin priors.

Ref. [66] computed similar Bayes factors for individual tabulated EOSs, finding $\ln B^{\rm BNS}_{\rm BBH} \lesssim 2$ in every case for their wide mass prior, with the majority of EOSs considered yielding $\ln B^{\rm BNS}_{\rm BBH} \sim 0$, in good agreement with our $\ln B^{\rm BNS}_{\rm BBH}(\chi_i \leq 0.89,\ \textit{agnostic}) = 0.85 \pm 0.69$.

Our calculations demonstrate that GW170817 is more consistent with a system containing at least one NS as compared to a BBH. Of course, this result is unsurprising given that an electromagnetic counterpart was observed. Assuming GW170817 was a BNS, we predict the amount of matter from dynamical ejecta available outside the remnant, similar in spirit to Refs. [26] and [99], among others [66, 82, 100–102]. Using the fitting formula reported in the appendix of Ref. [26], which depends primarily on stellar compactness, we estimate the amount of dynamical ejecta and its velocity, finding $M^{\rm (dyn)}_{\rm ejecta} = 6.5^{+6.3}_{-3.9} \times 10^{-3}$ $(3.9^{+2.4}_{-1.3} \times 10^{-3})$ $M_\odot$ and $v^{\rm (dyn)}_{\rm ejecta}/c = 0.257^{+0.027}_{-0.034}$ $(0.231^{+0.014}_{-0.014})$ with our *agnostic* (*informed*) prior, generally in good agreement with estimates of the contribution of dynamical ejecta in the literature. We note that our error bars only account for the residual EOS uncertainty, but modeling systematics associated with Ref. [26]'s fit surely contribute to the error budget as well. As has been previously noted, our finding suggests the dynamical ejecta were only a small part of the total ejecta of $\gtrsim 0.05\,M_\odot$ which powered GW170817's kilonova [26, 99].

Numerical relativity simulations typically do not extend far enough past merger to observe mass ejected via disk winds, which are expected to dominate the total ejected mass. Similarly, it is difficult to estimate the lanthanide fraction, which determines the opacity of the ejected material and the kilonova's color, from first principles based on M_1, M_2, and the EOS. However, were such models available, our posterior processes would immediately bound the expected kilonova properties, just as we already constrain the contribution of dynamical ejecta.

TABLE I. Medians *a posteriori* and highest-probability-density 90% credible regions for macroscopic observables and central densities associated with GW170817.

Prior ($\mathcal{H}_i$)	$M_1\,[M_\odot]$	$M_2\,[M_\odot]$	Λ_1	Λ_2	$\tilde{\Lambda}$	R_1 [km]	R_2 [km]	$\rho_{c,1}\,[10^{14}\,\mathrm{g/cm^3}]$	$\rho_{c,2}\,[10^{14}\,\mathrm{g/cm^3}]$
informed	$1.46^{+0.11}_{-0.10}$	$1.28^{+0.08}_{-0.09}$	380^{+249}_{-231}	844^{+553}_{-405}	572^{+254}_{-212}	$12.50^{+0.98}_{-0.87}$	$12.51^{+1.02}_{-0.96}$	$7.43^{+1.48}_{-1.23}$	$6.65^{+1.03}_{-1.04}$
agnostic	$1.49^{+0.13}_{-0.13}$	$1.25^{+0.11}_{-0.10}$	148^{+274}_{-125}	430^{+519}_{-301}	245^{+361}_{-160}	$10.88^{+1.99}_{-1.37}$	$10.82^{+2.14}_{-1.55}$	$9.79^{+3.21}_{-3.72}$	$8.85^{+2.52}_{-3.18}$

TABLE II. Posterior probabilities for progenitor systems assuming equal prior odds. We compare the evidence for a BNS, a NSBH (M_1 is a NS), a BHNS (M_1 is a BH), and a BBH. Monte-Carlo sampling uncertainties are approximately three orders of magnitude smaller than the point-estimates. Reported uncertainties approximate systematic error from our KDE model of the GW likelihood, which is largest for the BBH hypothesis.

Spin Prior	EOS Prior ($\mathcal{H}_i$)	$P(\mathrm{BNS}\|\mathrm{data};\mathcal{H}_i)$	$P(\mathrm{BHNS}\|\mathrm{data};\mathcal{H}_i)$	$P(\mathrm{NSBH}\|\mathrm{data};\mathcal{H}_i)$	$P(\mathrm{BBH}\|\mathrm{data};\mathcal{H}_i)$
$\lvert\chi_i\rvert \leq 0.05$	*informed*	$(14.3 \pm 4.5)\%$	$(23.6 \pm 0.5)\%$	$(54.4 \pm 1.2)\%$	$(7.8 \pm 2.7)\%$
	agnostic	$(25.9 \pm 7.1)\%$	$(27.6 \pm 1.8)\%$	$(38.3 \pm 2.2)\%$	$(8.1 \pm 3.1)\%$
$\lvert\chi_i\rvert \leq 0.89$	*informed*	$(11.2 \pm 3.7)\%$	$(18.1 \pm 0.1)\%$	$(61.0 \pm 0.3)\%$	$(9.7 \pm 3.3)\%$
	agnostic	$(23.9 \pm 6.9)\%$	$(25.2 \pm 1.4)\%$	$(40.4 \pm 1.7)\%$	$(10.5 \pm 3.9)\%$

IV. IMPLICATIONS FOR NEUTRON STAR PROPERTIES

In addition to examining the inferred properties of GW170817, we can use the GW data to inform our knowledge of NSs in general. Specifically, we compute posterior processes for various functional degrees of freedom, including the EOS itself and several derived relations between macroscopic observables. If all NSs share a single universal EOS, then these results are immediately applicable to other systems. Tight constraints on these relationships imply consistency tests of the universal-EOS hypothesis with observations of other systems [34, 103]. Tables III and IV summarize our conclusions, and we discuss a few salient points in more detail below. As in Section III, we report medians and 90% highest-probability-density credible regions unless otherwise noted.

A. Posterior processes for the EOS

We begin with an inference of the EOS itself, as shown in Figure 3. *A posteriori*, we observe a general trend towards lower pressures, particularly between ρ_{nuc} and $2\rho_{\mathrm{nuc}}$, with a trend back towards pressures near the *a priori* median at higher densities. Table III quantifies the uncertainty in pressure at a few reference densities.

The constraints we obtain are slightly different than, but consistent with, those reported in LE, which is expected from the differences in our GP EOS prior processes. Our *agnostic* and *informed* results bracket those reported in Ref. [13]'s parametric analysis, namely $p(2\rho_{\mathrm{nuc}}) = 3.5^{+2.7}_{-1.7} \times 10^{34}\ \mathrm{dyn/cm^2}$ and $p(6\rho_{\mathrm{nuc}}) = 9.0^{+7.9}_{-2.6} \times 10^{35}\ \mathrm{dyn/cm^2}$. Specifically, our *agnostic* results are systematically lower *a posteriori* than Ref. [13]'s, while our *informed* pressure bounds are centered above Ref. [13] at $2\rho_{\mathrm{nuc}}$. At $6\rho_{\mathrm{nuc}}$, however, our *informed* process lies below both Ref. [13] and our *agnostic* results, although the uncertainties are broad. This inversion likely occurs because GW170817 has little constraining power at high densities, but the *informed* results favor the presence of quark matter, which systematically softens *a priori* in this regime.

The trend toward low pressures between ρ_{nuc} and $2\rho_{\mathrm{nuc}}$ is likely driven by at least two factors. First, the NS radius and tidal deformability are known to correlate strongly with the pressure in that region [73, 104], and therefore GW170817's preference for small Λ manifests as a preference for lower pressures. However, GW170817's component masses likely have central densities below $10^{15}\,\mathrm{g/cm^3}$, and therefore the GW data only contains information about the EOS at densities lower than this. At significantly higher densities, then, the EOS posterior will tend to snap back towards the prior. That tendency is compounded by the requirement that all EOSs support $1.93\,M_\odot$ stars, which forces initially soft EOSs to stiffen at higher densities in order to support massive stars.

B. Posterior distributions and processes for macroscopic observables

1. Maximum mass and binding energy

Our posterior process for the EOS immediately yields a posterior distribution for the maximum mass of a nonrotating NS (M_{max}, sometimes called M_{TOV}). Like LE, we find that smaller M_{max} are preferred *a posteriori*, and that the shift is larger from prior to posterior for the *agnostic* result. This is consistent with the preference for softer EOSs, many of which struggle to support the $1.93\,M_\odot$ stars required *a priori* and therefore reach their M_{max} soon thereafter. We find $M_{\mathrm{max}} = 2.064^{+0.260}_{-0.134}$ ($2.017^{+0.238}_{-0.087}$) $M_\odot$ with the *agnostic* (*informed*) prior, broadly consistent with other constraints in the literature

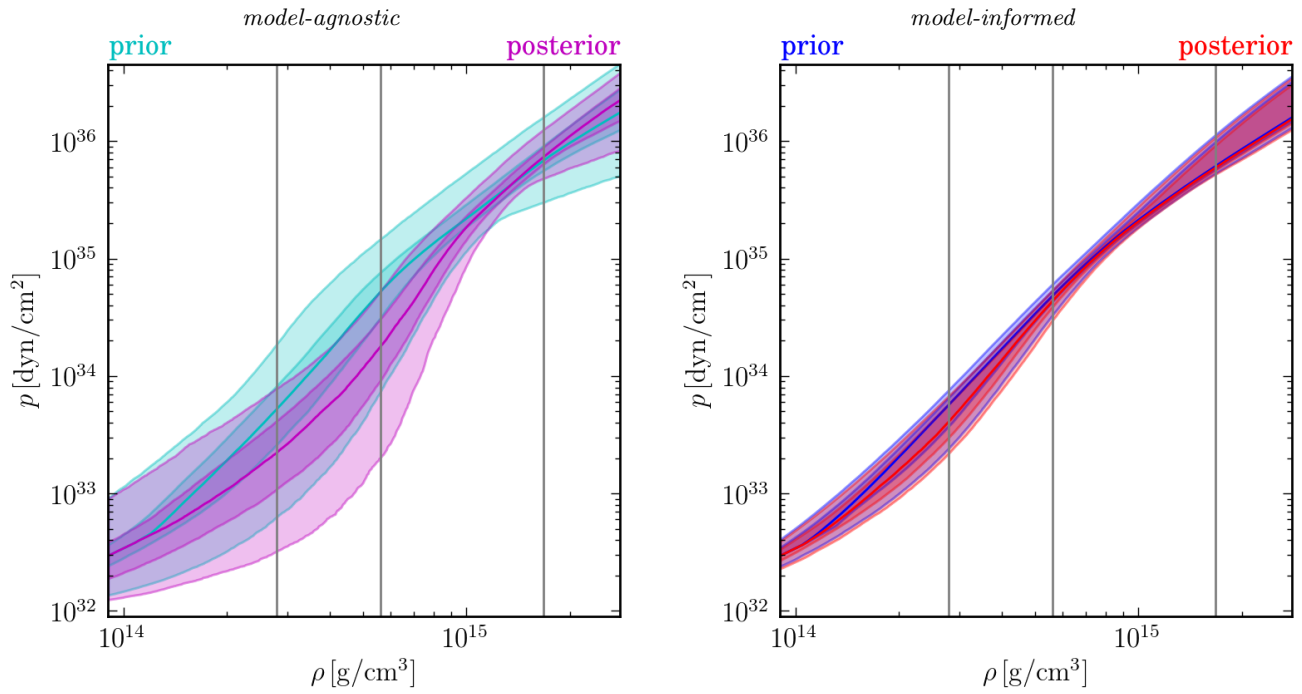

FIG. 3. EOS processes after marginalizing over composition. (*Left*) *model-agnostic* prior (*cyan*) and posterior (*magenta*) processes. (*Right*) *model-informed* prior (*blue*) and posterior (*red*) processes. Shaded regions correspond to 50% and 90% symmetric marginal credible regions for the pressure at each density. Solid lines denote the median and vertical lines denote $\rho_{\rm nuc}$, $2\rho_{\rm nuc}$, and $6\rho_{\rm nuc}$.

TABLE III. Medians *a posteriori* and highest-probability-density 90% credible regions for a canonical $1.4\,M_\odot$ NS's central density, and for pressures at several reference densities.

Prior ($\mathcal{H}_i$)	$\rho_{\rm c,1.4}\,[\mathrm{g/cm^3}]$	$p(\rho_{\rm nuc})\,[\mathrm{dyn/cm^2}]$	$p(2\rho_{\rm nuc})\,[\mathrm{dyn/cm^2}]$	$p(6\rho_{\rm nuc})\,[\mathrm{dyn/cm^2}]$
informed	$7.15^{+1.12}_{-1.04}\times10^{14}$	$4.25^{+0.76}_{-2.10}\times10^{33}$	$4.44^{+1.09}_{-1.34}\times10^{34}$	$6.84^{+5.58}_{-1.12}\times10^{35}$
agnostic	$9.40^{+2.78}_{-3.41}\times10^{14}$	$2.26^{+4.01}_{-2.14}\times10^{33}$	$1.81^{+2.80}_{-1.80}\times10^{34}$	$8.56^{+4.81}_{-3.88}\times10^{35}$

from both GW and EM data [22, 23, 27, 28, 31, 66], although there remains some disagreement about EM constraints in the literature (cf. Ref. [31]).

Such constraints may be put to the test as more NSs with large masses are discovered [38]. They could play an important role in the analysis of BHNS systems for which $\tilde{\Lambda}\sim(M_2/M_1)^4\Lambda_2$ can be quite small. Indeed, precise knowledge of $M_{\rm max}$ may be the best way to rule out the possibility that the lighter component is a NS, particularly if the source is distant enough that electromagnetic counterparts are unlikely to be detectable. It is worth noting that, while our *agnostic* posterior favors softer EOSs in the density regime relevant for GW170817, it produces looser $M_{\rm max}$ constraints than the *informed* posterior, supporting larger $M_{\rm max}$ than are allowed by the *informed* prior. This is associated with the additional model freedom within the *agnostic* prior, which allows the EOSs to vary significantly at densities larger than those occurring within GW170817's components.

Table IV also reports the baryonic mass $M_{b,1.4}$ of a canonical $1.4\,M_\odot$ NS. Besides its possible relevance for the amount of matter available to power electromagnetic counterparts, the difference between M_b and the NS mass defines the star's binding energy, with more compact stars corresponding to larger M_b at fixed M. GW170817 suggests that canonical NSs typically have binding energies of 0.15–$0.2\,M_\odot$, corresponding to $>10\%$ of the rest mass of their baryonic content. This is roughly consistent with predictions in the literature (e.g., Refs. [86, 106]). Figure 7 shows that there is significant overlap between our priors and posteriors for M_b, although there is a consistent trend toward more compact stars a posteriori, particularly with the *agnostic* prior.

2. *Mass-tidal deformability, mass-radius, and mass-moment of inertia relations*

Figure 4 shows our posterior processes for several macroscopic observables as a function of the NS mass. We generally find an *a posteriori* preference for smaller Λ, R, and I at a given M, consistent with relatively compact NSs. This preference is stronger with the *agnostic* posterior than the *informed*, again reflecting the *agnos-*

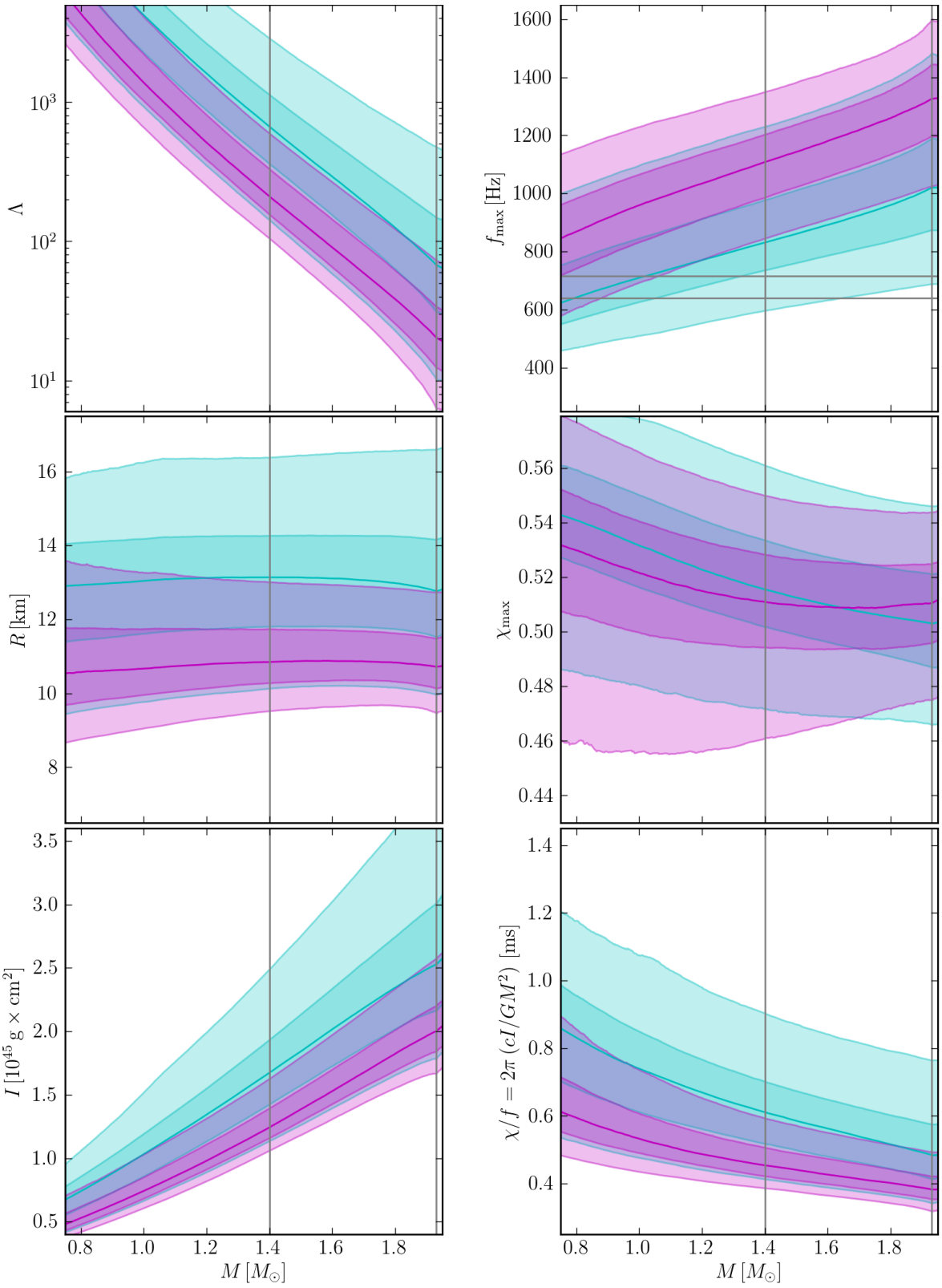

FIG. 4. Processes relating a few macroscopic observables after marginalizing over EOS composition with the *agnostic* prior. Prior (*cyan*) and posterior (*magenta*) processes for (*left*) tidal deformability (Λ; *top*), radius (R; *middle*), and moment of inertia (I; *bottom*) as functions of mass as well as (*right*) the maximum spin frequency ($f_{\max}$; *top*), maximum dimensionless spin parameter ($\chi_{\max}$; *middle*), and the dimensionless spin parameter divided by the spin frequency (*bottom*), useful when estimating χ for a pulsar with unknown mass. Shaded regions denote the 50% and 90% symmetric credible regions for the marginal distribution of each observable at each mass. Solid lines denote the median and vertical lines denote canonical $1.4\,M_\odot$ stars. Horizontal grey lines in the *top-right* panel denote the measured spin frequencies of J1748–2446ad (716 Hz [36]) and B1937+241 (641 Hz [105]), which lie below the 90% lower limits for $f_{\max}$ only when $M \gtrsim M_\odot$.

TABLE IV. Medians *a posteriori* and highest-probability-density 90% credible regions for a few canonical macroscopic quantities and for the maximum mass.

Prior ($\mathcal{H}_i$)	$\Lambda_{1.4}$	$R_{1.4}$ [km]	$I_{1.4}$ [10^{45} g cm^2]	$M_{b,1.4}$ [$M_\odot$]	$M_{\rm max}$ [$M_\odot$]
informed	491^{+216}_{-181}	$12.51^{+1.00}_{-0.88}$	$1.55^{+0.17}_{-0.16}$	$1.566^{+0.025}_{-0.021}$	$2.017^{+0.238}_{-0.087}$
agnostic	211^{+312}_{-137}	$10.86^{+2.04}_{-1.42}$	$1.25^{+0.35}_{-0.22}$	$1.591^{+0.049}_{-0.053}$	$2.064^{+0.260}_{-0.134}$

tic result's preference for particularly soft EOSs. Table IV quotes credible regions for a canonical $1.4\,M_\odot$ NS, showing good agreement with values reported elsewhere. LE bounded $\Lambda_{1.4}$ to lie between 47 and 608 (384 and 719) at 90% confidence whith their *agnostic* (*informed*) prior while Ref. [13] found $\Lambda_{1.4} = 190^{+390}_{-120}$. We find $\Lambda_{1.4} = 211^{+312}_{-137}$ (491^{+216}_{-181}).

Ref. [19] recently claimed $R_{1.4} = 11.0^{+0.9}_{-0.6}$ km based on GW170817 with a strongly theory-informed prior and a parameterization of the sound-speed at high densities [39, 43]. We note that their point-estimate is slightly larger than our *agnostic* result ($10.86^{+2.04}_{-1.42}$ km), but that their uncertainties are similar to our *informed* prior. Their result, then, is likely dependent on their *a priori* assumptions about the EOS, much like how our *informed* prior strongly influences the posterior constraints.

The derived relations as functions of mass, informed by GW170817, are likely to be of greatest relevance for future observations of both GW events and electromagnetic sources. For example, X-ray timing of pulsars is expected to constrain their masses and radii [51], radio observations of binary pulsars may measure NSs' moments of inertia [34, 63, 103], and additional GW observations of coalescing binary NSs should produce M–Λ measurements consistent with the current constraints [5, 41, 107]. These measurements will effectively act as a null-test of the hypothesis that all NSs share a single EOS, which is currently difficult to constrain with GW170817 alone (see Ref. [8] and errata of Ref. [9]). Indeed, the extreme model freedom allowed by nonparametric analyses will enable novel consistency tests and alternative hypotheses to compare against the universal-EOS assumption.

C. Maximum spin and asteroseismology

The EOS constraints derived from GW170817 have implications for the maximum NS spin, since the Keplerian breakup frequency $f_{\rm dyn} = \sqrt{GM/R^3}/2\pi$ is sensitive to the radius. Numerical studies of rapidly rotating NSs show that the maximum spin is typically $f_{\rm max} \sim 0.58 f_{\rm dyn}$, accurate to $\sim 7\%$, after accounting for spin-induced oblateness [108–111]. Here we report estimates for $f_{\rm max}$, and the corresponding maximum dimensionless spin $\chi_{\rm max} = cI(2\pi f_{\rm max})/GM^2$, as a function of mass. We note that our calculation for I assumes slowly rotating stars. Oblate, rapidly rotating stars will have larger I (possibly significantly larger [110, 112, 113]) and therefore our $\chi_{\rm max}$ should be interpreted as a lower limit. Previous studies [114, 115] noted that the maximum spin obtainable for any NS mass is significantly larger than the maximum observed spin frequency, currently 716 Hz [36]. We find consistent results, with $\max_M\{f_{\rm max}\} \gtrsim 1.4$ kHz. However, the maximum spin frequency at a particular mass can be significantly lower, perhaps by as much as a factor of two. What's more, the proximity of our lower bound on $f_{\rm max}$to the observed 716-Hz spin frequency for J1748–2446ad [36] may call into question the need for additional braking mechanisms [116–119] to limit the spin frequency of recycled millisecond pulsars.

The corresponding constraints on the maximum dimensionless spin ($\chi_{\rm max}$) demonstrate that NS spins must be $\lesssim 0.5$ for astrophysically plausible masses. This provides a natural upper bound on the NS spin prior for future Bayesian analyses if the observed distribution of spins in galactic binaries is not applicable to the broader population. Figure 4 also shows $\chi/f \equiv 2\pi cI/GM^2$ as a function of mass, from which we can compute the dimensionless spin of any pulsar given its observed rotation frequency, even if its mass is not precisely known, with the same caveats as $\chi_{\rm max}$ about rapid rotation. We do this for several pulsars with well-measured masses in Table V. In particular, the low-spin priors assumed in our work, as well as in Refs. [1, 8, 13, 66], are motivated by J0737−3039A and J1946+2052, with claims that their spins at merger would be below 0.04 and 0.05 [8], respectively. Our results, which assume $\chi \leq 0.05$ *a priori*, support this, with J0737–3039A's current spin inferred to be $0.021^{+0.006}_{-0.004}$ ($0.025^{+0.002}_{-0.002}$) with our *agnostic* (*informed*) priors. This is consistent with the dimensionless spin of $\chi \leq 0.034$ inferred for J0737–3039A via universal relations in Ref. [103] without the low-spin assumption.

Similarly, we also find the spin of J1807–2500B ($f = 238$ Hz [120]), one of the fastest pulsars with a well-measured mass, to be $0.11^{+0.03}_{-0.02}$ ($0.13^{+0.01}_{-0.01}$). Although the dimensionless spin of the fastest known pulsar (J1748–2446ad) depends on its unknown mass, we find $0.25 \leq \chi \leq 0.65$ for a wide, astrophysically plausible mass range. In fact, J1748–2446ad's spin frequency is consistent with $f \gtrsim f_{\rm max}/2$ at 90% confidence, regardless of mass, and is consistent with $f = f_{\rm max}$ at $> 90\%$ confidence with our *agnostic* prior if $M \lesssim 1.05\,M_\odot$.

Although beyond the scope of the current work, we also note that precise knowledge of the EOS determines the behavior of several dynamical tidal effects. The EOS determines the eigenmode spectrum within a NS, and therefore our posterior processes could be used to determine the exact placement and impact of linear resonant dynamical tidal effects due to f-modes and low-order g-modes during GW-driven inspirals (e.g.,

TABLE V. Inferred dimensionless spins for several pulsars with known masses with our *agnostic* (*informed*) composition-marginalized priors. J1807–2500 is a likely BNS, J0737−3039 is a known BNS, and J0348+0432 is a NS-white dwarf binary. The upper limits for J0737−3039A, in particular, support the low-spin priors assumed in this work and Refs. [1, 8, 13, 15, 66].

PSR	$M\,[M_\odot]$	f [Hz]	χ	
			agnostic	*informed*
J1807–2500B [120]	1.37	238.88	$0.1101^{+0.0317}_{-0.0187}$	$0.1319^{+0.0100}_{-0.0118}$
J0737–3039A [97]	1.34	44.05	$0.0205^{+0.0059}_{-0.0036}$	$0.0246^{+0.0019}_{-0.0022}$
J0348+0432 [37]	2.01	25.56	$0.0098^{+0.0023}_{-0.0017}$	$0.0107^{+0.0011}_{-0.0010}$

Refs. [121–124]). Similarly, knowledge of the r-mode spectrum could inform the Chandrasekhar-Friedman-Schutz (CFS) instabilities [125, 126] relevant for millisecond pulsars [114, 127, 128], and knowledge of the p- and g-mode spectra could improve models of non-linear, non-resonant secular fluid instabilities relevant during the GW inspiral [129–133]. The precise impact of these last two phenomena, however, also depends strongly on the instabilities' saturation, which themselves are highly uncertain and may prevent precise EOS constraints from making strong predictions about their impact on GW signals.

V. IMPLICATIONS FOR NEUTRON-STAR COMPOSITION

Finally, we turn to GW170817's implications for NS composition. Unlike previous sections, here we break down our *agnostic* and *informed* priors according to the composition of the EOSs upon which they were conditioned, presenting results separately for hadronic, hyperonic and quark GPs. More results for each composition are available in Appendix D.

To begin, we compare the evidence for each composition assuming both components were slowly spinning NSs. Table VI shows the posterior probabilities assuming equal prior odds. Notably, we find weak, but suggestive, evidence in favor of quark matter within NSs with the *informed* prior, although the *agnostic* prior prefers EOSs containing only hadrons by a similar amount. The relevance of hadronic vs. quark composition is less clear in the *agnostic* priors by design, though, as they resemble the input EOSs less closely. This is likely just a statement that the tabulated EOS from the literature containing quark matter are softer, on average, than those labeled either hadronic or hyperonic. It is also worth repeating that none of the compositions are overwhelmingly favored. Nonetheless, the preference for quark EOSs is tantalizing, as theoretical considerations suggest there should be a phase transition to quark matter at sufficiently high densities [134].

Regardless of the precise details of NS composition, another interesting question is whether there are strong first-order phase transitions within the EOS, leading to, e.g., distinct hadronic and quark phases of matter. One possible signature of such strong phase transitions is the existence of a disconnected hybrid star branch in the M-R relation. Stable sequences of NSs exist between critical points in the M-R relation; the first stable sequence is called the NS branch, and any subsequent branches at densities above the phase-transition onset are called hybrid star branches (see, e.g., Ref. [135]). A variety of hybrid star models have been proposed in the literature, motivated both on phenomenological grounds [136, 137] and by the possible existence of specific exotic phases [44, 135, 138–144], such as deconfined quark matter. While some models explicity include strong phase transitions, not all do. Regardless, previous analyses of hybrid stars have relied on parameterized EOS models of some kind. Our results are new in that they do not depend on an assumed functional form for the EOS nor do they build in any particular preference for the existence or absence of phase transitions *a priori*. Although the presence of only a single stable branch does not preclude the existence of phase transitions, multiple stable branches in the M-R relation constitute support for a strong first-order phase transition in the EOS. We compute Bayes factors comparing the evidence for EOSs that support multiple stable branches at central densities above $0.8\rho_{\rm nuc}$ to those with only a single stable branch above $0.8\rho_{\rm nuc}$ ($B^{n>1}_{n=1}$), finding weak evidence that favors multiple stable branches by a factor of 2 with our *agnostic* priors compared to the preference with pulsar data alone. Table VI shows the results for composition-marginalized priors, and the evidence ratios for each composition separately are of the same order of magnitude. While others have shown that GW170817 is not incompatible with hybrid stars, we are the first to rigorously quantify this preference. This is far from conclusive, but is suggestive of new physics within NS cores.

Pursuing this further, Figure 5 shows our *agnostic* prior and posterior processes conditioned on the number of stable branches above $0.8\rho_{\rm nuc}$. From this we see that, assuming the EOS supports at least one disconnected hybrid branch, GW170817 noticeably prefers EOSs that dramatically soften near $\rho_{\rm nuc}$ before stiffening significantly around $2\rho_{\rm nuc}$. While we expect this type of behavior within EOSs that have multiple stable branches, our priors do not have any particular preference for the phase transition to occur in this density range. Intriguingly, the central densities inferred for GW170817 (see Table I) suggest that any exotic particles associated with the putative phase transition around $\rho_{\rm nuc}$ would have been present

TABLE VI. Posterior probabilities for each composition assuming both components were slowly rotating NSs and equal prior odds, as well as Bayes factors for the number of stable branches in the mass-radius relation with the composition-marginalized priors. Monte-Carlo sampling uncertainties are approximately two orders of magnitude smaller than the point-estimates. The Bayes factor for the *informed* prior is unresolved because its standard deviation is much larger than the point-estimate.

Prior ($\mathcal{H}_i$)	P(Hadronic|data)	P(Hyperonic|data)	P(Quark|data)	$B^{n>1}_{n=1}$|Marginalized
informed	28%	16%	56%	unresolved
agnostic	50%	14%	36%	$2.0513 \pm (9.5 \times 10^{-3})$

within GW170817's components' cores before they coalesced. This finding is consistent with Ref. [141]'s conclusion that tidal deformability constraints from GW170817 cannot rule out the presence of a hybrid star. Figure 3 shows the processes regardless of the number of stable branches and is dominated by EOSs with a single stable branch since these are favored *a priori* by a factor of ~ 10. While we see the same general trend toward softer EOSs, this manifests as a general decrease in pressure at all densities, whereas there is a notable preference for softening and stiffening at specific densities when there are multiple stable branches.

We also note that the posterior preference for multiple stable branches depends on the precise lower limit of $M_{\rm max}$ allowed in our priors. The requirement that $M_{\rm max} \geq 1.93\,M_\odot$ forces the EOS to become stiff at high densities, thereby imparting the preference for EOSs that stiffen again after they initially soften. Without that requirement, EOSs that do not stiffen significantly (and hence support only a single stable branch) can still reproduce the GW170817 data reasonably well, weakening the modest preference for EOSs with multiple stable branches. We expect observations of more massive pulsars (e.g., [38]) to increase the preference for multiple stable branches, all else being equal.

While we stress that the statistical evidence in favor of EOSs that support multiple stable branches in the M-R relation is weak, GW170817's preference for soft EOSs, in conjunction with the existence of a 2 $M_\odot$ pulsar, could be interpreted as evidence for a strong phase transition between $\rho_{\rm nuc}$ and $2\rho_{\rm nuc}$, although the precise onset density, pressure, and latent energy associated with such a phase transition are still largely uncertain. Nonetheless, some theoretical studies of chiral effective field theory suggest that the purely hadronic model for the EOS will break down in this density range due to phase transitions [39, 40, 43, 81]. This coincidence is intriguing, especially since none of our input candidate EOSs are computed within the chiral effective field theory framework. It is therefore possible that we have observed exotic particles in the cores of coalescing NSs with GW170817.

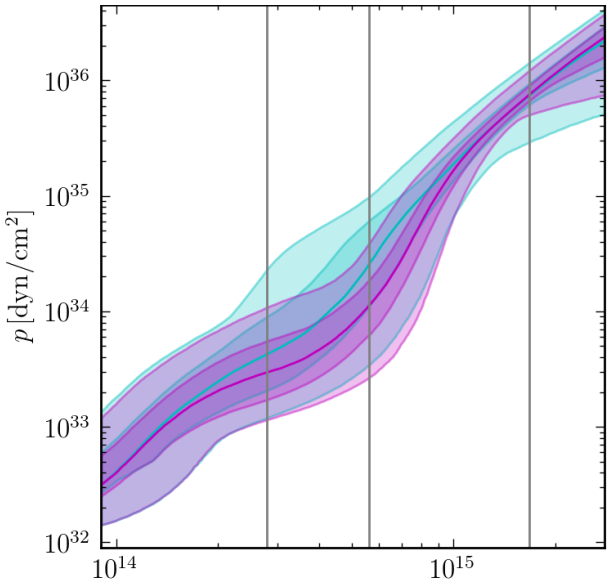

FIG. 5. *Agnostic* EOS prior (*cyan*) and posterior (*magenta*) processes for EOSs that support multiple stable branches in the M-R relation above $\rho_c = 0.8\rho_{\rm nuc}$ after marginalizing over composition. The equivalent processes for EOSs that support a single stable branch are indistinguishable from Figure 3. The general preference for softer EOSs *a posteriori* manifests as a dramatic softening at or below $\rho_{\rm nuc}$ before stiffening at approximately $2\rho_{\rm nuc}$. *Gray* lines denote $\rho_{\rm nuc}$, $2\rho_{\rm nuc}$, and $6\rho_{\rm nuc}$, respectively. Bayes factors between multiple and single stable branches for the agnostic priors are $B^{n>1}_{n=1} = 2.0513 \pm (9.5 \times 10^{-3})$, $1.5274 \pm (6.8 \times 10^{-3})$, $4.084 \pm (1.9 \times 10^{-2})$, and $1.684 \pm (1.7 \times 10^{-2})$ for the marginalized, hadronic, hyperonic, and quark compositions, respectively.

VI. DISCUSSION

We have presented a comprehensive nonparametric inference of the EOS of NS matter, as informed by GW170817 with refined GP EOS priors conditioned on a representative selection of candidate models from nuclear theory. By constructing separate priors for different underlying compositions of NS matter, we systematically investigated whether GW170817 prefers supranuclear matter with hadronic, hyperonic and/or quark constituents at the densities relevant for GWs. Intriguingly, we found a very weak preference for an EOS that supports quark matter with our *informed* prior. While other studies have hypothesized that GW170817 could have involved compact objects containing quark matter [44, 141–146], we are the first to make a quantitative evaluation of its likelihood and to examine the question outside of a specific parameterization or choice for the EOS.

We also found a marginal preference for EOSs that support multiple stable sequences in their M-R relation—i.e. a disconnected hybrid star branch, one possible signature of a strong phase transition—with our *agnostic* prior when comparing results based on GW and massive pulsar data against those from massive pulsar data alone. While this preference is too weak to be conclusive, we note that if the EOS does support hybrid stars, there is a noticeable propensity for dramatic softening around $\rho_{\rm nuc}$ followed by stiffening around $2\rho_{\rm nuc}$. This feature is consistent with a strong phase transition and its location agrees with chiral effective field theory predictions for the breakdown of the perturbed asymmetric nuclear matter description of the EOS [39, 40, 43, 81].

The possibility that GW170817 was a NSBH, rather than a BNS, has been discussed extensively in the literature [66, 147–150]. When examining only the GW data itself, we did not find a meaningful preference for either scenario. We did, however, find mild evidence against a BBH progenitor, with $B^{\rm NS}_{\rm BBH} = 3.3 \pm 1.4$, in accordance with analyses of individual tabulated EOSs [66] and the observation of electromagnetic counterparts [82, 83].

We also pointed out that the lower limit on the maximum spin frequency of NSs can approach the observed spin frequencies of some millisecond pulsars if they have relatively low masses ($\lesssim M_\odot$). Because the masses of many millisecond pulsars are unknown, this may warrant a reexamination of the need for additional braking mechanisms [116–119], such as r-mode CFS instabilities.

Because there is as yet only a limited amount of GW data to analyze (the recently announced GW190425 [151] contains little information about the EOS), the quantitative details of our results are undoubtedly sensitive to our choice of priors. We have consequently designed our training set of candidate EOSs to be as representative as possible by sampling widely from the literature. The prior dependence is additionally and explicitly mitigated by our *agnostic* GP, which is designed to include any EOS that satisfies basic physical requirements like causality and thermodynamic stability. At low densities, the pressure-density uncertainty bands calculated in chiral effective field theory [39, 40, 43, 81] could be helpful in producing priors with more direct theoretical motivation. At high densities, asymptotics from perturbative quantum chromodynamics (e.g. $c_s^2 \to c^2/3$ [152]) could similarly guide the design of our priors. Ultimately, however, it is new observational data that will drive precision and robustness gains in the EOS constraints. Of particular interest will be constraints from GW observations supplemented with X-ray measurements of NS masses and radii, such as the recent observations of J0030+0451 with NICER [153, 154], eventual radio measurements of double NS moments of inertia, and pulsar timing measurements of millisecond pulsar spin frequencies.

Nonparametric inference methods are well positioned to capitalize on these future observations because of their exquisite control of EOS modeling systematics and their broad coverage of varied EOS phenomenology. While our analysis is subject to systematic errors having to do with the finite number of posterior samples available in the GW data and with hard prior bounds in our KDE representations of the GW data, systematic uncertainties from such issues are currently dominated by statistical uncertainties, and will be for the foreseeable future. Additionally, the flexibility of our GPs could be further enhanced by using different covariance kernels, for example ones supporting different correlation length scales as a function of pressure. These improvements will be the subject of future work. Nonetheless, nonparametric inference has already proved to be a powerful tool when investigating ultra-dense matter. While the statistical evidence in favor of an exotic phase of matter within NS cores is marginal at best after GW170817, the agreement between some of our observations and predictions from nuclear theory is tantalizing and could prove to be the first faint indications of new physics at supranuclear densities.

ACKNOWLEDGMENTS

The authors gratefully acknowledge many useful discussions with Jocelyn Read, Maya Fishbach, Zoheyr Doctor, Amanda Farah, and Cole Miller, and also thank Armen Sedrakian for sharing several EOS tables. This research was partially completed while at the Kavli Institute for Theoretical Physics, and was supported in part by the NSF under grant NSF PHY11-25915. P. L. is supported in part by the Natural Sciences and Engineering Research Council of Canada, and by NSF grants PHY 15-05124 and PHY 17-08081 to the University of Chicago. R. E. and D. E. H. are supported at the University of Chicago by the Kavli Institute for Cosmological Physics through an endowment from the Kavli Foundation and its founder Fred Kavli. D. E. H. is also supported by NSF grant PHY-1708081, and gratefully acknowledges the Marion and Stuart Rice Award. The authors also gratefully acknowledge the computational resources provided by the LIGO Laboratory and supported by NSF grants PHY-0757058 and PHY-0823459.

[1] B. P. Abbott *et al.* (LIGO Scientific Collaboration and Virgo Collaboration), Phys. Rev. Lett. **119**, 161101 (2017), arXiv:1710.05832 [gr-qc].

[2] É. É. Flanagan and T. Hinderer, Phys. Rev. D **77**, 021502 (2008), arXiv:0709.1915 [astro-ph].

[3] T. Hinderer, B. D. Lackey, R. N. Lang, and J. S. Read, Phys. Rev. D **81**, 123016 (2010), arXiv:0911.3535 [astro-

ph.HE].
[4] J. S. Read, L. Baiotti, J. D. E. Creighton, J. L. Friedman, B. Giacomazzo, K. Kyutoku, C. Markakis, L. Rezzolla, M. Shibata, and K. Taniguchi, Phys. Rev. D **88**, 044042 (2013), arXiv:1306.4065 [gr-qc].
[5] W. Del Pozzo, T. G. F. Li, M. Agathos, C. Van Den Broeck, and S. Vitale, Phys. Rev. Lett. **111**, 071101 (2013).
[6] L. Wade, J. D. E. Creighton, E. Ochsner, B. D. Lackey, B. F. Farr, T. B. Littenberg, and V. Raymond, Phys. Rev. D **89**, 103012 (2014), arXiv:1402.5156 [gr-qc].
[7] T. Damour, A. Nagar, and L. Villain, Phys. Rev. D **85**, 123007 (2012), arXiv:1203.4352 [gr-qc].
[8] B. P. Abbott and et al., Physical Review X **9**, 011001 (2019), arXiv:1805.11579 [gr-qc].
[9] S. De *et al.*, Phys. Rev. Lett. **121**, 091102 (2018), arXiv:1804.08583 [astro-ph.HE].
[10] E. Annala, T. Gorda, A. Kurkela, and A. Vuorinen, Phys. Rev. Lett. **120**, 172703 (2018), arXiv:1711.02644 [astro-ph.HE].
[11] E. R. Most, L. R. Weih, L. Rezzolla, and J. Schaffner-Bielich, Phys. Rev. Lett. **120**, 261103 (2018), arXiv:1803.00549 [gr-qc].
[12] Y. Lim and J. W. Holt, Phys. Rev. Lett. **121**, 062701 (2018), arXiv:1803.02803 [nucl-th].
[13] B. P. Abbott and et al., Phys. Rev. Lett. **121**, 161101 (2018), arXiv:1805.11581 [gr-qc].
[14] A. Ayriyan, D. Alvarez-Castillo, D. Blaschke, and H. Grigorian, Universe **5**, 61 (2019), arXiv:1812.10796 [astro-ph.HE].
[15] P. Landry and R. Essick, Phys. Rev. D **99**, 084049 (2019), arXiv:1811.12529 [gr-qc].
[16] Y. Lim and J. W. Holt, European Physical Journal A **55**, 209 (2019), arXiv:1902.05502 [nucl-th].
[17] M. C. Miller, C. Chirenti, and F. K. Lamb, arXiv e-prints , arXiv:1904.08907 (2019), arXiv:1904.08907 [astro-ph.HE].
[18] Y. Zhou, L.-W. Chen, and Z. Zhang, Phys. Rev. D **99**, 121301 (2019), arXiv:1901.11364 [nucl-th].
[19] C. D. Capano, I. Tews, S. M. Brown, B. Margalit, S. De, S. Kumar, D. A. Brown, B. Krishnan, and S. Reddy, arXiv e-prints , arXiv:1908.10352 (2019), arXiv:1908.10352 [astro-ph.HE].
[20] J.-L. Jiang, S.-P. Tang, D.-S. Shao, M.-Z. Han, Y.-J. Li, Y.-Z. Wang, Z.-P. Jin, Y.-Z. Fan, and D.-M. Wei, Astrophys. J. **885**, 39 (2019), arXiv:1909.06944 [astro-ph.HE].
[21] A. Bauswein, O. Just, H.-T. Janka, and N. Stergioulas, Astrophys. J. Lett. **850**, L34 (2017), arXiv:1710.06843 [astro-ph.HE].
[22] B. Margalit and B. D. Metzger, ApJL **850**, L19 (2017), arXiv:1710.05938 [astro-ph.HE].
[23] M. Shibata, S. Fujibayashi, K. Hotokezaka, K. Kiuchi, K. Kyutoku, Y. Sekiguchi, and M. Tanaka, Phys. Rev. D **96**, 123012 (2017), arXiv:1710.07579 [astro-ph.HE].
[24] D. Radice, A. Perego, F. Zappa, and S. Bernuzzi, ApJL **852**, L29 (2018), arXiv:1711.03647 [astro-ph.HE].
[25] D. Radice and L. Dai, European Physical Journal A **55**, 50 (2019), arXiv:1810.12917 [astro-ph.HE].
[26] M. W. Coughlin *et al.*, Monthly Notices of the Royal Astronomical Society **480**, 3871 (2018), arXiv:1805.09371 [astro-ph.HE].
[27] M. Ruiz, S. L. Shapiro, and A. Tsokaros, Phys. Rev. D **97**, 021501 (2018), arXiv:1711.00473 [astro-ph.HE].
[28] L. Rezzolla, E. R. Most, and L. R. Weih, Astrophys. J. Lett. **852**, L25 (2018), arXiv:1711.00314 [astro-ph.HE].
[29] K. Kiuchi, K. Kyutoku, M. Shibata, and K. Taniguchi, Astrophys. J. Lett. **876**, L31 (2019), arXiv:1903.01466 [astro-ph.HE].
[30] M. W. Coughlin, T. Dietrich, B. Margalit, and B. D. Metzger, Mon. Not. R. Astron. Soc. **489**, L91 (2019), arXiv:1812.04803 [astro-ph.HE].
[31] M. Shibata, E. Zhou, K. Kiuchi, and S. Fujibayashi, Phys. Rev. D **100**, 023015 (2019), arXiv:1905.03656 [astro-ph.HE].
[32] A. W. Steiner, J. M. Lattimer, and E. F. Brown, Astrophys. J. **722**, 33 (2010), arXiv:1005.0811 [astro-ph.HE].
[33] F. Özel, D. Psaltis, T. Güver, G. Baym, C. Heinke, and S. Guillot, Astrophys. J. **820**, 28 (2016), arXiv:1505.05155 [astro-ph.HE].
[34] B. Kumar and P. Landry, Phys. Rev. D **99**, 123026 (2019), arXiv:1902.04557 [gr-qc].
[35] M. Fasano, T. Abdelsalhin, A. Maselli, and V. Ferrari, Phys. Rev. Lett. **123**, 141101 (2019), arXiv:1902.05078 [astro-ph.HE].
[36] J. W. T. Hessels, S. M. Ransom, I. H. Stairs, P. C. C. Freire, V. M. Kaspi, and F. Camilo, Science **311**, 1901 (2006), arXiv:astro-ph/0601337 [astro-ph].
[37] J. Antoniadis *et al.*, Science **340**, 448 (2013), arXiv:1304.6875 [astro-ph.HE].
[38] H. T. Cromartie *et al.*, Nature Astronomy , 439 (2019), arXiv:1904.06759 [astro-ph.HE].
[39] I. Tews, J. Carlson, S. Gandolfi, and S. Reddy, Astrophys. J. **860**, 149 (2018), arXiv:1801.01923 [nucl-th].
[40] I. Tews, J. Margueron, and S. Reddy, The European Physical Journal A **55**, arXiv:1901.09874 (2019), arXiv:1901.09874 [nucl-th].
[41] M. Agathos, J. Meidam, W. Del Pozzo, T. G. F. Li, M. Tompitak, J. Veitch, S. Vitale, and C. Van Den Broeck, Phys. Rev. D **92**, 023012 (2015), arXiv:1503.05405 [gr-qc].
[42] C. A. Raithel, F. Özel, and D. Psaltis, Astrophys. J. Lett. **857**, L23 (2018), arXiv:1803.07687 [astro-ph.HE].
[43] I. Tews, J. Margueron, and S. Reddy, Phys. Rev. C **98**, 045804 (2018), arXiv:1804.02783 [nucl-th].
[44] C.-M. Li, Y. Yan, J.-J. Geng, Y.-F. Huang, and H.-S. Zong, Phys. Rev. D **98**, 083013 (2018), arXiv:1808.02601 [nucl-th].
[45] J. Aasi *et al.* (LIGO Scientific Collaboration), Class. Quantum Grav. **32**, 074001 (2015), arXiv:1411.4547 [gr-qc].
[46] F. Acernese *et al.* (Virgo Collaboration), Class. Quantum Grav. **32**, 024001 (2015), arXiv:1408.3978 [gr-qc].
[47] The LIGO Scientific Collaboration and The Virgo Collaboration, "Ligo/virgo s190425z: Identification of a gw compact binary merger candidate," https://gcn.gsfc.nasa.gov/gcn3/24168.gcn3 (2019).
[48] The LIGO Scientific Collaboration and The Virgo Collaboration, "Ligo/virgo s190814bv: Identification of a gw compact binary merger candidate," https://gcn.gsfc.nasa.gov/gcn3/25324.gcn3 (2019).
[49] B. D. Lackey and L. Wade, Phys. Rev. D **91**, 043002 (2015), arXiv:1410.8866 [gr-qc].
[50] M. McNeil Forbes, S. Bose, S. Reddy, D. Zhou, A. Mukherjee, and S. De, arXiv e-prints ,

arXiv:1904.04233 (2019), arXiv:1904.04233 [astro-ph.HE].
[51] K. C. Gendreau, Z. Arzoumanian, and T. Okajima, in *Proc. SPIE*, Society of Photo-Optical Instrumentation Engineers (SPIE) Conference Series, Vol. 8443 (2012) p. 844313.
[52] P. S. Ray, B. F. Phlips, K. S. Wood, D. Chakrabarty, R. A. Remillard, and C. A. Wilson-Hodge, arXiv e-prints , arXiv:1109.1309 (2011), arXiv:1109.1309 [astro-ph.IM].
[53] M. Feroci *et al.*, Experimental Astronomy **34**, 415 (2012), arXiv:1107.0436 [astro-ph.IM].
[54] P. S. Ray *et al.*, in *Proc. SPIE*, Society of Photo-Optical Instrumentation Engineers (SPIE) Conference Series, Vol. 10699 (2018) p. 1069919, arXiv:1807.01179 [astro-ph.IM].
[55] S. Zhang *et al.*, Science China Physics, Mechanics, and Astronomy **62**, 29502 (2019), arXiv:1812.04020 [astro-ph.IM].
[56] K. H. Lo, M. C. Miller, S. Bhattacharyya, and F. K. Lamb, Astrophys. J. **776**, 19 (2013), arXiv:1304.2330 [astro-ph.HE].
[57] D. Psaltis, F. Özel, and D. Chakrabarty, Astrophys. J. **787**, 136 (2014), arXiv:1311.1571 [astro-ph.HE].
[58] F. Özel, D. Psaltis, Z. Arzoumanian, S. Morsink, and M. Bauböck, Astrophys. J. **832**, 92 (2016), arXiv:1512.03067 [astro-ph.HE].
[59] A. L. Watts *et al.*, Reviews of Modern Physics **88**, 021001 (2016), arXiv:1602.01081 [astro-ph.HE].
[60] A. G. Lyne, M. Burgay, M. Kramer, A. Possenti, R. N. Manchester, F. Camilo, M. A. McLaughlin, D. R. Lorimer, N. D'Amico, B. C. Joshi, J. Reynolds, and P. C. C. Freire, Science **303**, 1153 (2004), arXiv:astro-ph/0401086 [astro-ph].
[61] J. M. Lattimer and B. F. Schutz, Astrophys. J. **629**, 979 (2005), arXiv:astro-ph/0411470 [astro-ph].
[62] M. Kramer and N. Wex, Classical and Quantum Gravity **26**, 073001 (2009).
[63] P. E. Dewdney, P. J. Hall, R. T. Schilizzi, and T. J. L. W. Lazio, IEEE Proceedings **97**, 1482 (2009).
[64] R. Nan, D. Li, C. Jin, Q. Wang, L. Zhu, W. Zhu, H. Zhang, Y. Yue, and L. Qian, International Journal of Modern Physics D **20**, 989 (2011), arXiv:1105.3794 [astro-ph.IM].
[65] C. G. Bassa, G. H. Janssen, R. Karuppusamy, M. Kramer, K. J. Lee, K. Liu, J. McKee, D. Perrodin, M. Purver, S. Sanidas, R. Smits, and B. W. Stappers, Mon. Not. R. Astron. Soc. **456**, 2196 (2016), arXiv:1511.06597 [astro-ph.IM].
[66] The LIGO Scientific Collaboration and et al., arXiv e-prints , arXiv:1908.01012 (2019), arXiv:1908.01012 [gr-qc].
[67] M. F. Carney, L. E. Wade, and B. S. Irwin, Phys. Rev. D **98**, 063004 (2018), arXiv:1805.11217 [gr-qc].
[68] L. Lindblom, Phys. Rev. D **98**, 043012 (2018), arXiv:1807.02538 [astro-ph.HE].
[69] S. K. Greif, G. Raaijmakers, K. Hebeler, A. Schwenk, and A. L. Watts, Mon. Not. R. Astron. Soc. **485**, 5363 (2019), arXiv:1812.08188 [astro-ph.HE].
[70] Z. F. Seidov, Soviet Ast. **15**, 347 (1971).
[71] J. L. Zdunik and P. Haensel, Astron. Astrophys. **551**, A61 (2013), arXiv:1211.1231 [astro-ph.SR].
[72] M. G. Alford, S. Han, and M. Prakash, Phys. Rev. D **88**, 083013 (2013), arXiv:1302.4732 [astro-ph.SR].
[73] J. S. Read, B. D. Lackey, B. J. Owen, and J. L. Friedman, Phys. Rev. D **79**, 124032 (2009), arXiv:0812.2163 [astro-ph].
[74] K. Hebeler, J. M. Lattimer, C. J. Pethick, and A. Schwenk, Astrophys. J. **773**, 11 (2013), arXiv:1303.4662 [astro-ph.SR].
[75] L. Lindblom, Phys. Rev. D **82**, 103011 (2010), arXiv:1009.0738 [astro-ph.HE].
[76] L. Lindblom and N. M. Indik, Phys. Rev. D **86**, 084003 (2012), arXiv:1207.3744 [astro-ph.HE].
[77] L. Lindblom and N. M. Indik, Phys. Rev. D **89**, 064003 (2014), arXiv:1310.0803 [astro-ph.HE].
[78] L. Lindblom, Phys. Rev. D **97**, 123019 (2018), arXiv:1804.04072 [astro-ph.HE].
[79] See, e.g., concerns over modeling errors within Ref. [10] and discussion of piecewise polytropic and spectral parameterizations within Ref. [13].
[80] R. Gamba, J. S. Read, and L. E. Wade, arXiv e-prints , arXiv:1902.04616 (2019), arXiv:1902.04616 [gr-qc].
[81] R. J. Furnstahl, N. Klco, D. R. Phillips, and S. Wesolowski, Phys. Rev. C **92**, 024005 (2015).
[82] B. P. Abbott and et al., Astrophys. J. Lett. **848**, L12 (2017), arXiv:1710.05833 [astro-ph.HE].
[83] B. P. Abbott and et al., Astrophys. J. Lett. **848**, L13 (2017), arXiv:1710.05834 [astro-ph.HE].
[84] LIGO Scientific Collaboration and Virgo Collaboration, "Properties of the Binary Neutron Star Merger GW170817," `https://dcc.ligo.org/LIGO-P1800061/public`.
[85] C. E. Rasmussen and C. K. I. Williams, *Gaussian Processes for Machine Learning* (The MIT Press, 2006).
[86] F. Douchin and P. Haensel, A&A **380**, 151 (2001), arXiv:astro-ph/0111092 [astro-ph].
[87] It is important to note that the sound speed in our final synthetic EOSs does not remain at ϕ_0 below the point at which we match to the crust.
[88] K. Hebeler, J. M. Lattimer, C. J. Pethick, and A. Schwenk, Astrophys. J. **773**, 11 (2013), arXiv:1303.4662 [astro-ph.SR].
[89] I. Tews, T. Krüger, K. Hebeler, and A. Schwenk, Phys. Rev. Lett. **110**, 032504 (2013), arXiv:1206.0025 [nucl-th].
[90] E. S. Fraga, A. Kurkela, and A. Vuorinen, European Physical Journal A **52**, 49 (2016), arXiv:1508.05019 [nucl-th].
[91] A. Kurkela, E. S. Fraga, J. Schaffner-Bielich, and A. Vuorinen, Astrophys. J. **789**, 127 (2014), arXiv:1402.6618 [astro-ph.HE].
[92] L. Engvik, E. Osnes, M. Hjorth-Jensen, G. Bao, and E. Ostgaard, Astrophys. J. **469**, 794 (1996), arXiv:nucl-th/9509016 [nucl-th].
[93] G. Baym, S. Furusawa, T. Hatsuda, T. Kojo, and H. Togashi, arXiv e-prints , arXiv:1903.08963 (2019), arXiv:1903.08963 [astro-ph.HE].
[94] B. P. Abbott *et al.* (LIGO Scientific Collaboration and Virgo Collaboration), Phys. Rev. X **9**, 031040 (2019).
[95] These samples were generated with uniform (flat) priors in M_1, M_2, Λ_1, and Λ_2, and therefore are drawn from a distribution proportional to the likelihood, which is what we model in our analysis.
[96] While our *informed* priors constrain R and $\tilde{\Lambda}$ more tightly, we note that Refs. [13] and [9] are more sim-

ilar to our *agnostic* prior and therefore consider this the relevant comparison.

[97] A. G. Lyne, M. Burgay, M. Kramer, A. Possenti, R. N. Manchester, F. Camilo, M. A. McLaughlin, D. R. Lorimer, N. D'Amico, B. C. Joshi, J. Reynolds, and P. C. C. Freire, Science **303**, 1153 (2004), arXiv:astro-ph/0401086 [astro-ph].

[98] K. Stovall *et al.*, Astrophys. J. Lett. **854**, L22 (2018), arXiv:1802.01707 [astro-ph.HE].

[99] B. P. Abbott and et al., Astrophys. J. Lett. **850**, L39 (2017), arXiv:1710.05836 [astro-ph.HE].

[100] D. Kasen, B. Metzger, J. Barnes, E. Quataert, and E. Ramirez-Ruiz, Nature (London) **551**, 80 (2017), arXiv:1710.05463 [astro-ph.HE].

[101] P. S. Cowperthwaite *et al.*, Astrophys. J. Lett. **848**, L17 (2017), arXiv:1710.05840 [astro-ph.HE].

[102] V. A. Villar, J. Guillochon, E. Berger, B. D. Metzger, P. S. Cowperthwaite, M. Nicholl, K. D. Alexander, P. K. Blanchard, R. Chornock, T. Eftekhari, W. Fong, R. Margutti, and P. K. G. Williams, Astrophys. J. Lett. **851**, L21 (2017), arXiv:1710.11576 [astro-ph.HE].

[103] P. Landry and B. Kumar, Astrophys. J. Lett. **868**, L22 (2018), arXiv:1807.04727 [gr-qc].

[104] J. M. Lattimer and M. Prakash, Astrophys. J. **550**, 426 (2001), arXiv:astro-ph/0002232 [astro-ph].

[105] D. C. Backer, S. R. Kulkarni, C. Heiles, M. M. Davis, and W. M. Goss, Nature (London) **300**, 615 (1982).

[106] E. Chabanat, P. Bonche, P. Haensel, J. Meyer, and R. Schaeffer, Nucl. Phys. A **627**, 710 (1997).

[107] B. D. Lackey and L. Wade, Phys. Rev. D **91**, 043002 (2015).

[108] G. B. Cook, S. L. Shapiro, and S. A. Teukolsky, Astrophys. J. **424**, 823 (1994).

[109] P. Haensel, M. Salgado, and S. Bonazzola, Astron. Astrophys. **296**, 745 (1995).

[110] V. Paschalidis and N. Stergioulas, Living Reviews in Relativity **20** (2017), 10.1007/s41114-017-0008-x.

[111] J. M. Lattimer and M. Prakash, Science **304**, 536 (2004), arXiv:astro-ph/0405262 [astro-ph].

[112] O. Benhar, V. Ferrari, L. Gualtieri, and S. Marassi, Phys. Rev. D **72**, 044028 (2005).

[113] Bejger, M., A&A **552**, A59 (2013).

[114] D. Chakrabarty, E. H. Morgan, M. P. Muno, D. K. Galloway, R. Wijnands, M. van der Klis, and C. B. Markwardt, Nature (London) **424**, 42 (2003), arXiv:astro-ph/0307029 [astro-ph].

[115] D. Chakrabarty, in *Binary Radio Pulsars*, Astronomical Society of the Pacific Conference Series, Vol. 328, edited by F. A. Rasio and I. H. Stairs (2005) p. 279, arXiv:astro-ph/0408004 [astro-ph].

[116] L. Bildsten, Astrophys. J. Lett. **501**, L89 (1998), arXiv:astro-ph/9804325 [astro-ph].

[117] C. Cutler, Phys. Rev. D **66**, 084025 (2002), arXiv:gr-qc/0206051 [gr-qc].

[118] N. Andersson, K. Kokkotas, and B. F. Schutz, Astrophys. J. **510**, 846 (1999), arXiv:astro-ph/9805225 [astro-ph].

[119] Y. Levin and G. Ushomirsky, Mon. Not. R. Astron. Soc. **324**, 917 (2001), arXiv:astro-ph/0006028 [astro-ph].

[120] R. S. Lynch, P. C. C. Freire, S. M. Ransom, and B. A. Jacoby, Astrophys. J. **745**, 109 (2012), arXiv:1112.2612 [astro-ph.HE].

[121] D. Lai, Mon. Not. R. Astron. Soc. **270**, 611 (1994), arXiv:astro-ph/9404062 [astro-ph].

[122] H. Yu and N. N. Weinberg, Mon. Not. R. Astron. Soc. **464**, 2622 (2017), arXiv:1610.00745 [astro-ph.HE].

[123] H. Yu and N. N. Weinberg, Mon. Not. R. Astron. Soc. **470**, 350 (2017), arXiv:1705.04700 [astro-ph.HE].

[124] W. Xu and D. Lai, Phys. Rev. D **96**, 083005 (2017), arXiv:1708.01839 [astro-ph.HE].

[125] S. Chandrasekhar, Phys. Rev. Lett. **24**, 611 (1970).

[126] J. L. Friedman and B. F. Schutz, Astrophys. J. **222**, 281 (1978).

[127] P. Arras, E. E. Flanagan, S. M. Morsink, A. K. Schenk, S. A. Teukolsky, and I. Wasserman, Astrophys. J. **591**, 1129 (2003), arXiv:astro-ph/0202345 [astro-ph].

[128] P. Arras, in *Binary Radio Pulsars*, Astronomical Society of the Pacific Conference Series, Vol. 328, edited by F. A. Rasio and I. H. Stairs (2005) p. 317.

[129] N. N. Weinberg, P. Arras, and J. Burkart, Astrophys. J. **769**, 121 (2013), arXiv:1302.2292 [astro-ph.SR].

[130] T. Venumadhav, A. Zimmerman, and C. M. Hirata, Astrophys. J. **781**, 23 (2014), arXiv:1307.2890 [astro-ph.HE].

[131] N. N. Weinberg, Astrophys. J. **819**, 109 (2016), arXiv:1509.06975 [astro-ph.SR].

[132] R. Essick, S. Vitale, and N. N. Weinberg, Phys. Rev. D **94**, 103012 (2016), arXiv:1609.06362 [astro-ph.HE].

[133] B. P. Abbott and et al., Phys. Rev. Lett. **122**, 061104 (2019), arXiv:1808.08676 [astro-ph.HE].

[134] G. Baym, T. Hatsuda, T. Kojo, P. D. Powell, Y. Song, and T. Takatsuka, Reports on Progress in Physics **81**, 056902 (2018), arXiv:1707.04966 [astro-ph.HE].

[135] K. Schertler, C. Greiner, J. Schaffner-Bielich, and M. H. Thoma, Nucl. Phys. A **677**, 463 (2000), arXiv:astro-ph/0001467 [astro-ph].

[136] U. H. Gerlach, Physical Review **172**, 1325 (1968).

[137] N. K. Glendenning and C. Kettner, Astron. Astrophys. **353**, L9 (2000), arXiv:astro-ph/9807155 [astro-ph].

[138] B. Kampfer, Journal of Physics A Mathematical General **14**, L471 (1981).

[139] M. Alford and A. Sedrakian, Phys. Rev. Lett. **119**, 161104 (2017), arXiv:1706.01592 [astro-ph.HE].

[140] D. E. Alvarez-Castillo and D. B. Blaschke, Phys. Rev. C **96**, 045809 (2017), arXiv:1703.02681 [nucl-th].

[141] V. Paschalidis, K. Yagi, D. Alvarez-Castillo, D. B. Blaschke, and A. Sedrakian, Phys. Rev. D **97**, 084038 (2018), arXiv:1712.00451 [astro-ph.HE].

[142] R. Nandi and P. Char, Astrophys. J. **857**, 12 (2018), arXiv:1712.08094 [astro-ph.HE].

[143] G. F. Burgio, A. Figura, H. J. Schulze, and J. B. Wei, arXiv e-prints , arXiv:1907.03283 (2019), arXiv:1907.03283 [nucl-th].

[144] G. Montaña, L. Tolós, M. Hanauske, and L. Rezzolla, Phys. Rev. D **99**, 103009 (2019), arXiv:1811.10929 [astro-ph.HE].

[145] G. F. Burgio, H. J. Schulze, and J. B. Wei, Nuclear and Particle Physics Proceedings **306-308**, 61 (2019).

[146] H. Gieg, T. Dietrich, and M. Ujevic, arXiv e-prints , arXiv:1908.03135 (2019), arXiv:1908.03135 [gr-qc].

[147] H. Yang, W. E. East, and L. Lehner, Astrophys. J. **856**, 110 (2018), arXiv:1710.05891 [gr-qc].

[148] M. W. Coughlin and T. Dietrich, Phys. Rev. D **100**, 043011 (2019), arXiv:1901.06052 [astro-ph.HE].

[149] T. Hinderer, S. Nissanke, F. Foucart, K. Hotokezaka, T. Vincent, M. Kasliwal, P. Schmidt, A. R. Williamson, D. A. Nichols, M. D. Duez, L. E. Kidder, H. P. Pfeiffer, and M. A. Scheel, Phys. Rev. D **100**, 063021 (2019),

arXiv:1808.03836 [astro-ph.HE].
[150] F. Foucart, M. D. Duez, L. E. Kidder, S. M. Nissanke, H. P. Pfeiffer, and M. A. Scheel, Phys. Rev. D **99**, 103025 (2019), arXiv:1903.09166 [astro-ph.HE].
[151] B. P. Abbott *et al.*, arXiv e-prints , arXiv:2001.01761 (2020), arXiv:2001.01761 [astro-ph.HE].
[152] A. Kurkela, P. Romatschke, and A. Vuorinen, Phys. Rev. D **81**, 105021 (2010), arXiv:0912.1856 [hep-ph].
[153] M. C. Miller *et al.*, Astrophys. J. Lett. **887**, L24 (2019), arXiv:1912.05705 [astro-ph.HE].
[154] T. E. Riley *et al.*, Astrophys. J. Lett. **887**, L21 (2019), arXiv:1912.05702 [astro-ph.HE].
[155] S. Goriely, N. Chamel, and J. M. Pearson, Phys. Rev. C **82**, 035804 (2010), arXiv:1009.3840 [nucl-th].
[156] S. Goriely, N. Chamel, and J. M. Pearson, Phys. Rev. C **88**, 024308 (2013).
[157] B. K. Agrawal, Phys. Rev. C **81**, 034323 (2010), arXiv:1003.3295 [nucl-th].
[158] S. Banik, M. Hempel, and D. Bandyopadhyay, Astrophys. J. Suppl. **214**, 22 (2014), arXiv:1404.6173 [astro-ph.HE].
[159] T. Gaitanos, M. Di Toro, S. Typel, V. Baran, C. Fuchs, V. Greco, and H. H. Wolter, Nucl. Phys. A **732**, 24 (2004), arXiv:nucl-th/0309021 [nucl-th].
[160] G. A. Lalazissis, T. Nikšić, D. Vretenar, and P. Ring, Phys. Rev. C **71**, 024312 (2005).
[161] N. K. Glendenning and S. A. Moszkowski, Phys. Rev. Lett. **67**, 2414 (1991).
[162] F. Gulminelli and A. R. Raduta, Phys. Rev. C **92**, 055803 (2015), arXiv:1504.04493 [nucl-th].
[163] B. K. Agrawal, S. Shlomo, and V. K. Au, Phys. Rev. C **72**, 014310 (2005), arXiv:nucl-th/0505071 [nucl-th].
[164] H. Müther, M. Prakash, and T. L. Ainsworth, Physics Letters B **199**, 469 (1987).
[165] G. A. Lalazissis, J. König, and P. Ring, Phys. Rev. C **55**, 540 (1997), arXiv:nucl-th/9607039 [nucl-th].
[166] J. Friedrich and P. G. Reinhard, Phys. Rev. C **33**, 335 (1986).
[167] B. K. Agrawal, S. Shlomo, and V. Kim Au, Phys. Rev. C **68**, 031304 (2003), arXiv:nucl-th/0308042 [nucl-th].
[168] P. G. Reinhard and H. Flocard, Nucl. Phys. A **584**, 467 (1995).
[169] W. Nazarewicz, J. Dobaczewski, T. R. Werner, J. A. Maruhn, P. G. Reinhard, K. Rutz, C. R. Chinn, A. S. Umar, and M. R. Strayer, Phys. Rev. C **53**, 740 (1996).
[170] L. Bennour, P. H. Heenen, P. Bonche, J. Dobaczewski, and H. Flocard, Phys. Rev. C **40**, 2834 (1989).
[171] P. G. Reinhard, D. J. Dean, W. Nazarewicz, J. Dobaczewski, J. A. Maruhn, and M. R. Strayer, Phys. Rev. C **60**, 014316 (1999), arXiv:nucl-th/9903037 [nucl-th].
[172] E. Chabanat, *Interactions effectives pour des conditions extrêmes d'isospin*, Theses, Université Claude Bernard - Lyon I (1995).
[173] Y. Sugahara and H. Toki, Nucl. Phys. A **579**, 557 (1994).
[174] M. Fortin, C. Providência, A. R. Raduta, F. Gulminelli, J. L. Zdunik, P. Haensel, and M. Bejger, Phys. Rev. C **94**, 035804 (2016), arXiv:1604.01944 [astro-ph.SR].
[175] M. E. Gusakov, P. Haensel, and E. M. Kantor, Mon. Not. R. Astron. Soc. **439**, 318 (2014), arXiv:1401.2827 [astro-ph.HE].
[176] B. D. Lackey, M. Nayyar, and B. J. Owen, Phys. Rev. D **73**, 024021 (2006), arXiv:astro-ph/0507312 [astro-ph].
[177] M. Alford, M. Braby, M. Paris, and S. Reddy, Astrophys. J. **629**, 969 (2005), arXiv:nucl-th/0411016 [nucl-th].
[178] L. Bonanno and A. Sedrakian, Astron. Astrophys. **539**, A16 (2012), arXiv:1108.0559 [astro-ph.SR].

Appendix A: Details of nonparametric prior construction

While Section II provides an overview of how we construct our priors, we report many important technical details here. First, as in LE, each tabulated $\varepsilon(p)$ is resampled to obtain a process for $\phi(p)$ using $K_{\rm se}$ and $K_{\rm wn}$ with hyperparameters optimized separately for each EOS. Because the data for each tabulated EOS represents a single function, we optimize hyperparameters using the marginal likelihood (see Section 5.4.1 of [85])

$$\log P_{\rm ML}(\varepsilon|p,\vec{\sigma}) = -\frac{1}{2}(\varepsilon_i-\mu_i)\left(K^{-1}\right)_{ij}(\varepsilon_j-\mu_j) - \frac{N}{2}\log(2\pi) - \frac{1}{2}\log|K_{ij}| \quad \text{(A1)}$$

where N is the dimensionality of ε_i and $|K_{ij}|$ is the determinant of the covariance matrix. This likelihood, which is the probability of obtaining the observed data given a GP with the specified hyperparameters, selects the best-fit element of the statistical model defined by our GP. We typically observe strong correlations between σ and l, as increasing either increases the correlation between neighboring points.

We note that EOSs with sharp features, like strong first-order phase transitions, are somewhat difficult to model with a squared-exponential kernel because $K_{\rm se}$ strictly generates analytic functions. Nonetheless, we find it is still possible to adequately represent the behavior seen in, e.g., tabulated EOSs that contain quark matter over the densities relevant for GW170817.

We then construct separate GPs to represent all tabulated EOSs belonging to the same composition and family using $K_{\rm se}$, $K_{\rm wn}$, and $K_{\rm mv}$. Because these GPs are meant to emulate the typical behavior of a group of proposed EOSs rather than reproduce a single function, we select hyperparameters based on a cross-validation likelihood (see Section 5.4.2 of [85] and Eq. (10)). The cross-validation likelihood selects hyperparameters that produce synthetic EOSs with a variance similar to what is seen between elements of the training set. We select a single set of optimal hyperparameters based on the cross-validation likelihood separately for each composition and family.

Similar to $P_{\rm ML}$, $P_{\rm CV}$ shows strong correlations between σ and l. These are often independent of $\sigma_{\rm obs}$ and m, which themselves show strong degeneracies. Usually, the input EOSs strongly prefer a specific (σ, l) pair, indicative of the typical correlations and length scales in the underlying data. Additionally, the cross-validation requires at least some spread in the conditioned processes,

meaning that as long as either $\sigma_{\rm obs}$ or m is sufficiently large, there is little preference for the precise combination.

After obtaining GPs for each composition and family combination, we construct *agnostic* and *informed* GPs for each composition, both of which are conditioned on the GPs for all families within that composition. Each family is weighed equally so that those containing many slightly different tabulated EOSs are not more strongly weighed than families with fewer EOSs, as the number of tabulated EOSs in each family may depend on different authors' propensities to publish. We note that this is not a unique choice and different relative weights would produce different priors.

As described in Section II A, we again use the cross-validation likelihood (Eq 10) with $K_{\rm se}$, $K_{\rm wn}$, and $K_{\rm mv}$ to obtain processes that emulate the behavior seen within each composition, observing similar correlations to those observed within each combination of composition and family. However, instead of selecting a single set of hyperparameters, we sample from $P_{\rm CV}$ as in Eq. 11. This generates a mixture model of many different GPs from which we sample when drawing from our priors.

We generate *informed* priors via simulated annealing, repeatedly Monte-Carlo sampling from the hyperprior as we slowly decrease the temperature in order to find the high-likelihood portions of hyperparameter space. However, we note that taking the limit $T \to \infty$ with arbitrary prior bounds may not produce the range of variability desired for the *agnostic* prior. Specifically, we identify several regions of hyperparameter space that produce nearly identical conditioned processes, several of which we consider "too tight" as they do not produce a broad range of synthetic EOSs. Therefore, we impose several additional hyperprior constraints for the *agnostic* priors. We require $\sigma \geq 1$, $\sigma_{\rm obs} \geq 1$, $m \geq 1$, and $(\sigma_{\rm obs}^2 + m^2) \geq 2\sigma^2$. The first condition allows the resulting processes to deviate significantly from the mean, while the second and third conditions make the conditioned process less sensitive to the specific behavior seen in the tabulated EOSs. The final condition on the ratio of hyperparameters avoids situations where the modeling uncertainty ($\sigma_{\rm obs}$, m) is significantly smaller than the marginal $K_{\rm se}$ uncertainty (σ). When that happens, the conditioned process returns a weighed average of the input EOSs with a variance similar to the modeling uncertainty rather than σ, as would be expected when taking the average of many independent Gaussian-distributed variates. In the opposite extreme, where the modeling uncertainty is much larger than σ, the resulting conditioned process follows the prior mean with variances characteristic of σ, which produce reasonably broad synthetic EOSs because we require $\sigma \geq 1$. We additionally allow l to vary over nearly an order of magnitude.

Appendix B: Optimal Gaussian kernel density estimate representations of the gravitational-wave likelihood

Our Gaussian KDE model for the GW likelihood is constructed in the four-dimensional space spanned by M_1, M_2, Λ_1, and Λ_2. We assume a diagonal covariance (C_{ij}) within our Gaussian kernels, optimizing the bandwidths directly by varying a scale parameter for each dimension's sample variance so that

$$C_{ij} = b^2\sigma_i^2\delta_{ij} \quad \Big| \quad \sigma_i^2 = \frac{1}{N}\sum_\alpha \left(x_i^{(\alpha)}\right)^2 - \left(\frac{1}{N}\sum_\alpha x_i^{(\alpha)}\right)^2 \tag{B1}$$

Pragmatically, this is done by whitening the samples with the sample variance in each dimension separately and then optimizing a scale parameter for a covariance proportional to the identity matrix. This is achieved by directly maximizing a leave-one-out cross-validation likelihood as a function of the scale parameter b

$$\log L_{\rm CV} = \sum_i^N \log\left(\frac{1}{N-1}\sum_{j\neq i}^{N-1} k(x_i, x_j; b)\right) \tag{B2}$$

where k is our multi-dimensional Gaussian kernel. Using the available samples [84], we find optimal bandwidths of $b_{\rm opt} = 0.1247$ (0.0905) for the low-spin (high-spin) data set.

Furthermore, to account for hard prior bounds like $\Lambda_{1,2} \geq 0$, we reflect our samples across such boundaries, *de facto* forcing the KDE's derivative to vanish at the boundary in directions perpendicular to the boundary. This can introduce systematic biases beyond those produced by the smoothing inherent in all KDE models. We measure the scale of their impact on Monte-Carlo integrals conducted along the boundary by comparing estimates with and without reflected samples. Note that the relative weight assigned to samples far from the boundary, i.e. most of the BNS Monte-Carlo points, are virtually unaffected by such issues, and these primarily concern NSBH, BHNS, and BBH models.

Appendix C: Tabulated equations of state used to condition nonparametric priors

Table VII lists the tabulated candidate EOSs used to condition our nonparametric priors, including their $M_{\rm max}$ and source references.

Appendix D: Supplementary figures and tables

We present a few additional tables and figures relevant for our analyses. Tables VIII-X contain results broken down by composition. Figure 6 shows *informed*-prior

TABLE VII. Tabulated EOSs grouped in the same way we construct our priors, first by combining members of each family of underlying nuclear effective forces separately, and then combining separate families for each composition.

Composition	Family	Moniker	$M_{\max}$ $[M_\odot]$	Reference
Hadronic	BSK	bsk20	2.16	[155]
		bsk21	2.27	
		bsk22	2.26	[156]
		bsk23	2.27	
		bsk24	2.28	
		bsk25	2.22	
		bsk26	2.15	
	BSR	bsr2	2.38	[157]
		bsr6	2.43	
	DD	dd2	2.42	[158]
		ddhd	2.14	[159]
		ddme2	2.48	[160]
	ENG	eng	2.24	[92]
	GM	gm1	2.36	[161]
	KDE	kde0v	1.96	[162]
		kde0v1	1.97	[163]
	MPA	mpa1	2.46	[164]
	NL	nl3	2.77	[165]
	R	rs	2.12	[166]
	SK	sk255	2.14	[167]
		sk272	2.23	
		ski2	2.16	[168]
		ski3	2.24	
		ski4	2.17	
		ski5	2.24	
		ski6	2.19	[169]
		skmp	2.11	[170]
		skop	1.97	[171]
	SLY	sly230a	2.10	[106]
		sly2	2.05	[172]
		sly9	2.16	
		sly	2.05	[86]
	TM	tm1	2.18	[173]

Composition	Family	Moniker	$M_{\max}$ $[M_\odot]$	Reference
Hyperonic	BSR	bsr2y	2.00	[174]
		bsr6y	2.02	
	DD	dd2y	2.00	[174]
		ddme2y	2.09	
	GM	gm1b	1.99	[175]
		gm1y	2.02	[174]
	H	h4	2.03	[176]
	NL	nl3y	2.31	[174]
	TM	tm1c	2.06	[175]
Quark	ALF	alf2	2.09	[177]
		alf4	1.94	
	DDQ	ddq0625	1.93	[178]
		ddq0630	2.07	
		ddq0825	1.99	
		ddq0830	2.08	
	HQC	hqc18	2.05	[93]
		hqc19	2.07	

results for functional relations between generic NS observables, and Figure 7 plots distributions for canonical quantities and the maximum mass.

TABLE VIII. Medians *a posteriori* and highest-probability-density 90% credible regions for macroscopic observables associated with GW170817, with priors broken down according to the composition of the EOSs upon which they were conditioned.

Prior ($\mathcal{H}_i$)		$M_1\,[M_\odot]$	$M_2\,[M_\odot]$	Λ_1	Λ_2	$\tilde{\Lambda}$	R_1 [km]	R_2 [km]	$\rho_{c,1}\,[10^{14}\,\mathrm{g/cm^3}]$	$\rho_{c,2}\,[10^{14}\,\mathrm{g/cm^3}]$
informed	Hadronic	$1.45^{+0.10}_{-0.09}$	$1.28^{+0.08}_{-0.08}$	444^{+222}_{-250}	961^{+532}_{-382}	658^{+188}_{-156}	$12.96^{+0.57}_{-0.55}$	$13.03^{+0.55}_{-0.57}$	$7.07^{+1.10}_{-0.99}$	$6.41^{+0.77}_{-0.85}$
	Hyperonic	$1.46^{+0.08}_{-0.09}$	$1.28^{+0.08}_{-0.07}$	502^{+294}_{-187}	1114^{+495}_{-414}	760^{+131}_{-150}	$13.20^{+0.39}_{-0.43}$	$13.28^{+0.34}_{-0.45}$	$7.02^{+0.87}_{-0.91}$	$6.19^{+0.71}_{-0.65}$
	Quark	$1.46^{+0.12}_{-0.10}$	$1.27^{+0.08}_{-0.10}$	315^{+210}_{-179}	742^{+425}_{-328}	496^{+145}_{-166}	$12.14^{+0.63}_{-0.68}$	$12.10^{+0.59}_{-0.76}$	$7.83^{+1.44}_{-1.30}$	$6.94^{+1.06}_{-0.94}$
agnostic	Hadronic	$1.50^{+0.13}_{-0.13}$	$1.25^{+0.11}_{-0.10}$	124^{+181}_{-103}	379^{+402}_{-257}	216^{+266}_{-141}	$10.66^{+1.66}_{-1.35}$	$10.59^{+1.79}_{-1.57}$	$10.38^{+3.35}_{-3.76}$	$9.36^{+2.59}_{-3.21}$
	Hyperonic	$1.47^{+0.12}_{-0.11}$	$1.27^{+0.10}_{-0.09}$	268^{+324}_{-229}	690^{+600}_{-522}	466^{+337}_{-337}	$12.14^{+1.39}_{-1.90}$	$12.15^{+1.44}_{-2.07}$	$8.29^{+3.51}_{-2.48}$	$7.32^{+3.11}_{-1.96}$
	Quark	$1.49^{+0.13}_{-0.12}$	$1.25^{+0.10}_{-0.10}$	162^{+260}_{-135}	456^{+483}_{-310}	262^{+335}_{-162}	$10.94^{+1.80}_{-1.27}$	$10.84^{+1.88}_{-1.45}$	$9.46^{+3.02}_{-3.52}$	$8.55^{+2.41}_{-2.90}$

TABLE IX. Medians *a posteriori* and highest-probability-density 90% credible regions for a few canonical macroscopic quantities, with priors broken down according to the composition of the EOSs upon which they were conditioned.

Prior ($\mathcal{H}_i$)		$\Lambda_{1.4}$	$R_{1.4}$ [km]	$I_{1.4}\,[10^{45}\,\mathrm{g\,cm^2}]$	$M_{b,1.4}\,[M_\odot]$	$M_{\max}\,[M_\odot]$
informed	Hadronic	561^{+163}_{-137}	$12.98^{+0.55}_{-0.56}$	$1.61^{+0.12}_{-0.11}$	$1.552^{+0.010}_{-0.010}$	$2.233^{+0.098}_{-0.098}$
	Hyperonic	650^{+113}_{-134}	$13.23^{+0.37}_{-0.43}$	$1.67^{+0.08}_{-0.10}$	$1.589^{+0.008}_{-0.007}$	$2.017^{+0.071}_{-0.084}$
	Quark	427^{+125}_{-143}	$12.14^{+0.59}_{-0.72}$	$1.50^{+0.11}_{-0.14}$	$1.568^{+0.017}_{-0.016}$	$1.978^{+0.082}_{-0.048}$
agnostic	Hadronic	185^{+228}_{-119}	$10.65^{+1.69}_{-1.42}$	$1.21^{+0.29}_{-0.21}$	$1.591^{+0.055}_{-0.057}$	$2.091^{+0.272}_{-0.161}$
	Hyperonic	399^{+296}_{-285}	$12.15^{+1.37}_{-1.99}$	$1.47^{+0.26}_{-0.34}$	$1.602^{+0.048}_{-0.024}$	$2.038^{+0.225}_{-0.108}$
	Quark	228^{+291}_{-140}	$10.91^{+1.83}_{-1.31}$	$1.28^{+0.33}_{-0.20}$	$1.588^{+0.046}_{-0.052}$	$2.042^{+0.242}_{-0.112}$

TABLE X. Medians *a posteriori* and highest-probability-density 90% credible regions for canonical central densities and pressures at reference densities, with priors broken down according to the composition of the EOSs upon which they were conditioned.

Prior ($\mathcal{H}_i$)		$\rho_{c,1.4}\,[\mathrm{g/cm^3}]$	$p(\rho_{\mathrm{nuc}})\,[\mathrm{dyn/cm^2}]$	$p(2\rho_{\mathrm{nuc}})\,[\mathrm{dyn/cm^2}]$	$p(6\rho_{\mathrm{nuc}})\,[\mathrm{dyn/cm^2}]$
informed	Hadronic	$6.87^{+0.85}_{-0.84}\times10^{14}$	$6.07^{+1.29}_{-1.29}\times10^{33}$	$4.71^{+0.96}_{-0.84}\times10^{34}$	$11.81^{+1.45}_{-1.46}\times10^{35}$
	Hyperonic	$6.71^{+0.72}_{-0.64}\times10^{14}$	$5.86^{+1.03}_{-1.01}\times10^{33}$	$4.84^{+0.59}_{-0.66}\times10^{34}$	$6.70^{+0.64}_{-0.60}\times10^{35}$
	Quark	$7.47^{+1.15}_{-1.02}\times10^{14}$	$3.18^{+1.35}_{-1.24\times10^{33}}$	$4.06^{+1.14}_{-1.28}\times10^{34}$	$6.55^{+0.87}_{-0.89}\times10^{35}$
agnostic	Hadronic	$9.95^{+2.96}_{-3.36}\times10^{14}$	$2.09^{+4.25}_{-1.97}\times10^{33}$	$1.54^{+2.21}_{-1.53}\times10^{34}$	$9.50^{+5.12}_{-3.45}\times10^{35}$
	Hyperonic	$7.89^{+3.27}_{-2.17}\times10^{14}$	$4.22^{+2.80}_{-3.71}\times10^{33}$	$3.34^{+2.09}_{-3.10}\times10^{34}$	$7.18^{+3.43}_{-2.63}\times10^{35}$
	Quark	$9.07^{+2.73}_{-3.09}\times10^{14}$	$1.91^{+3.58}_{-1.78}\times10^{33}$	$1.87^{+2.87}_{-1.85}\times10^{34}$	$7.84^{+3.93}_{-3.59}\times10^{35}$

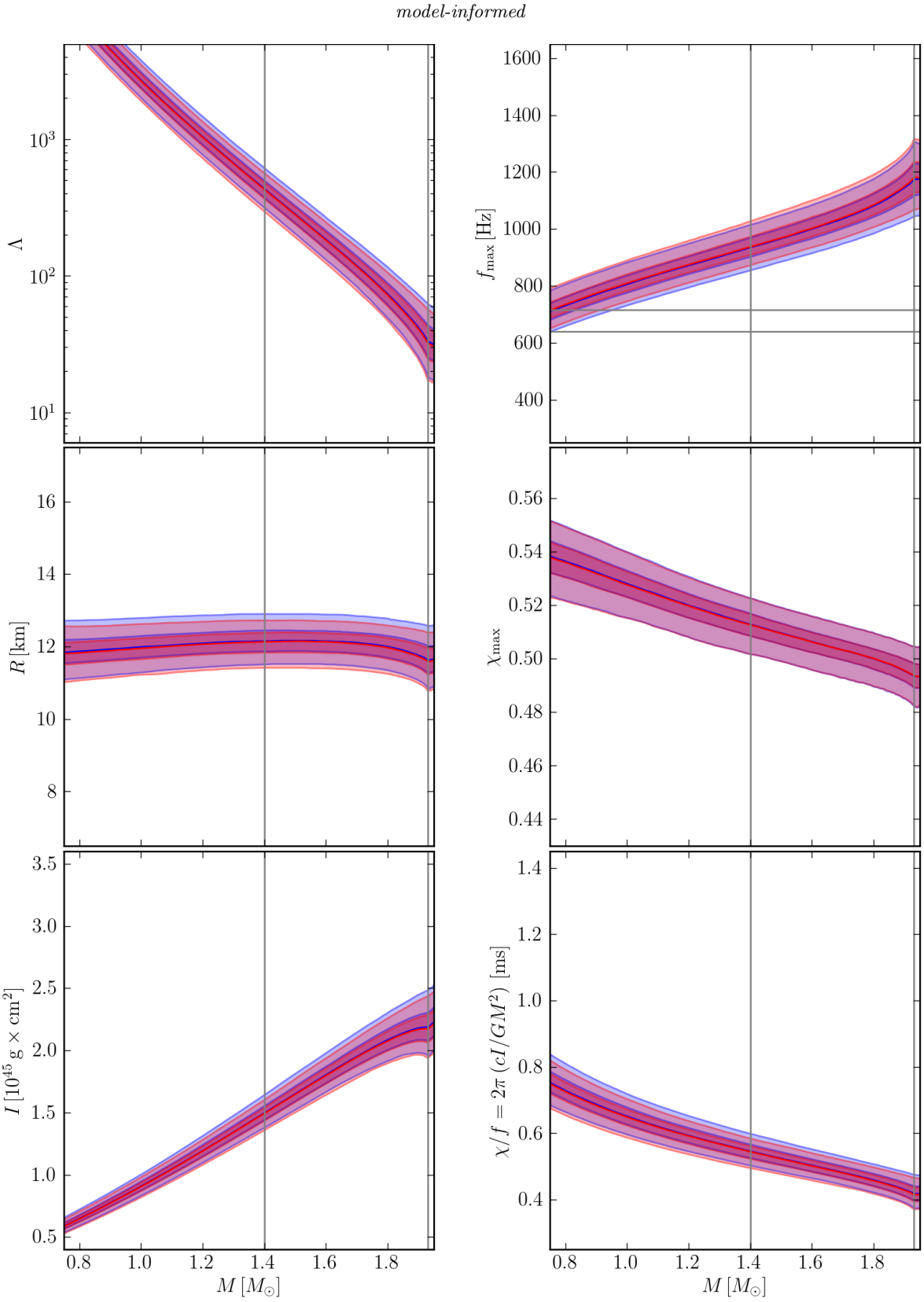

FIG. 6. Processes relating a few macroscopic observables after marginalizing over EOS-composition with the *informed* prior. Prior (*blue*) and posterior (*red*) processes for (*left*) tidal deformability (Λ; *top*), radius (R; *middle*), and moment-of-inertia (I; *bottom*) as functions of mass as well as (*right*) the maximum spin frequency ($f_{\rm max}$; *top*), maximum dimensionless spin parameter ($\chi_{\rm max}$; *middle*), and χ/f (*bottom*). Shaded regions denote the 50% and 90% symmetric credible regions for the marginal distribution of each observable at each mass. Solid lines denote the median and vertical lines denote canonical $1.4\,M_\odot$ stars. Horizontal grey lines in the *top-right* panel denote the measured spin frequencies of J1748–2446ad (716 Hz [36]) and B1937+241 (641 Hz [105]), which lie below but near the lower limits for $f_{\rm max}$.

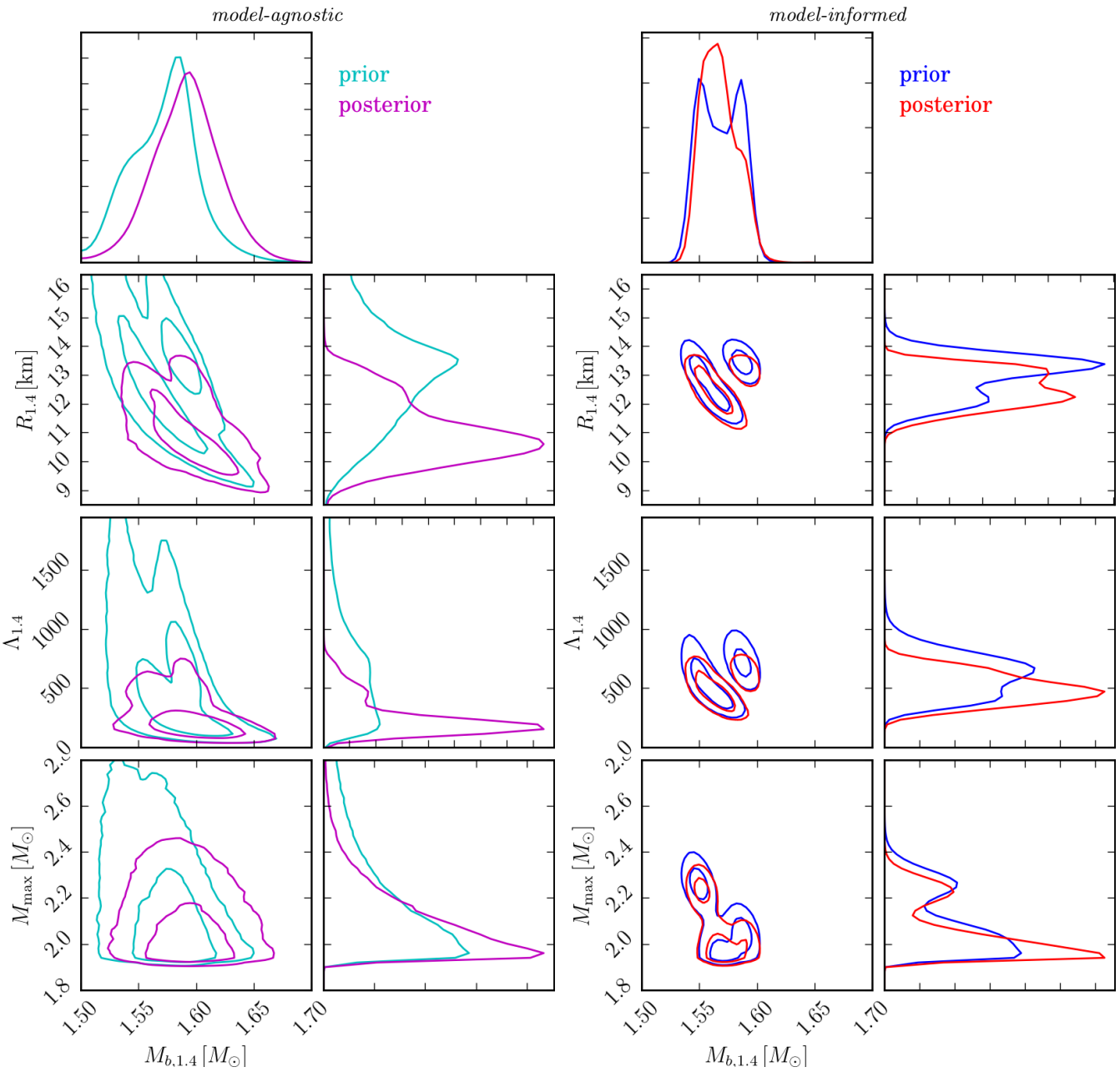

FIG. 7. Distributions for $M_{b,1.4}$, $M_{\rm max}$, $\Lambda_{1.4}$, and $R_{1.4}$ after marginalizing over EOS-composition. (*Left*) *model-agnostic* prior (*cyan*) and posterior (*magenta*). (*Right*) *model-informed* prior (*blue*) and posterior (*red*). Contours in the joint distributions denote minimal 50% and 90% credible regions. The bimodal behavior seen with the *agnostic* posterior is a combination of the inherited multimodal likelihood from GW170817 (see Figure 11 of Ref. [8]) as well as the preference for multiple stable branches. EOSs with multiple stable branches in the M-R relation *only* inhabit the low-$R_{1.4}$ mode, for example, while EOSs with a single stable branch inhabit both. The multimodal behavior seen with the *informed* prior is mostly due to the tight constraints imposed for each composition separately, which result in the separate peaks observed in these canonical observables.